Weak enforcement of interface continuity and generalized periodicity in high-order electromechanical problems

J. Barceló-Mercader[1] | D. Codony[2] | S. Fernández-Méndez[1] | I. Arias*[1,2]

[1]Laboratori de Càlcul Numèric (LaCàN), Universitat Politècnica de Catalunya (UPC), Campus Nord UPC-C2, E-08034 Barcelona, Spain

[2]Centre Internacional de Mètodes Numèrics en Enginyeria (CIMNE), 08034 Barcelona, Spain

Correspondence
*Irene Arias, Department of Civil and Environmental Engineering, School of Civil Engineering, Universitat Politècnica de Catalunya, Jordi Girona 1-3, Barcelona 08034. Email: irene.arias@upc.edu

Summary

We present a formulation for the weak enforcement of continuity conditions at material interfaces in high-order problems by means of Nitsche's method, which is particularly suited for unfitted discretizations. This formulation is extended to impose generalized periodicity conditions at the unit cell boundaries of periodic structures. The formulation is derived for flexoelectricity, a high-order electromechanical coupling between strain gradient and electric field, mathematically modelled as a coupled system of fourth-order PDEs. The design of flexoelectric devices requires the solution of high-order boundary value problems on complex material architectures, including general multimaterial arrangements. This can be efficiently achieved with an immersed boundary B-splines approach. Furthermore, the design of flexoelectric metamaterials also involves the analysis of periodic unit cells with generalized periodicity conditions. Optimal high-order convergence rates are obtained with an unfitted B-spline approximation, confirming the reliability of the method. The numerical simulations illustrate the usefulness of the proposed approach towards the design of functional electromechanical multi-material devices and metamaterials harnessing the flexoelectric effect.

KEYWORDS:
Nitsche's method, material interfaces, periodicity, high-order PDEs, flexoelectricity, unfitted discretization, immersed boundary

1 | INTRODUCTION

The numerical solution of boundary value problems involving systems of high-order partial differential equations (PDE) requires either (1) specialized finite elements compatible with C^0 approximations, such as mixed methods [1] and interior penalty methods [2], or (2) approximations based on smooth basis functions. In mixed finite elements, the primal field variables and their derivatives are interpolated as independent variables with C^0 basis functions. Mixed finite elements have been successfully used in strain-gradient elasticity [3] or Cahn-Hilliard equation [4]. They suffer however from stability issues and from cumbersome model-dependent implementations, as well as from a higher computational cost due to the large number of additional unknowns. C^0 penalty methods also consider standard C0 finite element approximations and impose the required continuity across elements weakly.

The approach to high-order PDE based on smooth basis functions is much more direct and only requires the approximation of the primal fields. The drawback is that it is, in general, more difficult to define smooth approximation spaces. One option is to

use meshfree methods, which easily enable local refinement[5,6]. However, these methods are very expensive due to quadrature and to the large sparsity pattern resulting from the significant overlap of basis functions required in higher-order problems. Furthermore, the treatment of boundary conditions on curved and non-convex geometries can be cumbersome. Another option is Isogeometric analysis (IGA) based on B-splines or NURBS[7]. Isogeometric methods describe boundary geometry with high fidelity and can deal with high-order PDE, but are too rigid in the bulk, e.g. to model composites. B-spline approximations in higher dimensions are constructed from tensor products and thus rely on cartesian meshes, incompatible in principle with general boundary geometries. This limitation can be circumvented by combining B-Splines with immersed boundary methods, which use meshes non-conforming to the boundary of the domain. This boundary is defined independently of the background mesh, and thus immersed boundary methods overcome the rigidity of tensor product B-Spline approximates[8]. In immersed boundary methods, essential boundary conditions cannot be enforced strongly since the basis functions are not interpolant at the boundary, and are often enforced weakly through Nitsche's method[9,10]. Similarly, continuity conditions at material interfaces or generalized periodic conditions at fictitious boundaries cannot be imposed strongly. Although continuity conditions for classic elasticity at material interfaces with Isogeometric analysis (IGA) have been developed[11,12], high-order interfaces in unfitted discretizations have not been addressed in the literature to the best of our knowledge.

Here, we present a formulation for the weak imposition of high-order interface conditions by means of Nitsche's method. We focus on flexoelectricity, a high-order electromechanical coupling that has received increasing attention in the last decades[13,14,15,16,17]. It refers to a universal property of all dielectrics, by which they produce an electric signal when subject to large mechanical field gradients, e.g. under bending at microscopic scales, and conversely they deform under the application of an inhomogeneous electric field. Mathematically, the governing equations of flexoelectricity form a coupled system of fourth-order PDEs for the mechanical displacement and the electric potential. Being a universal property, flexoelectricity provides a route to broaden the class of materials that can be used for electromechanical transduction beyond the limited class of piezoelectric materials. Nevertheless, harnessing flexoelectricity as a functional property in metamaterials and devices requires strain-gradient and polarization-gradient engineering, in particular through material inhomogeneities and complex material architectures. For this, the ability to solve flexoelectricity boundary value problems in general geometries and with general multi-material arrangements is crucial. Furthermore, the ability to study periodic lattice architectures is essential towards the design of flexoelectric metamaterials[18,19]. Several numerical methods for the solution of the flexoelectricity fourth-order system of PDEs have been proposed, including finite element solutions based on mixed formulations[20,21], finite differences[22,23], C^0 interior penalty finite element methods[24], and methods based on smooth approximations, such as maximum entropy meshless methods[25,26,27,28] and isogeometric approaches[29]. None of these methods, however, are capable of solving flexoelectric boundary value problems on complex geometries with high geometric fidelity. We recently proposed an immersed boundary hierarchical B-Spline-based method for the efficient solution of flexoelectricity and strain-gradient elasticity boundary value problem on arbitrarily shaped domains and electrode configurations[8]. Here, we extend this framework to flexoelectric problems with general physical or fictitious interfaces, with applications to material interfaces and generalized periodicity conditions.

Although the formulation is derived in the context of a B-spline immersed boundary method for flexoelectricity and strain-gradient elasticity boundary value problems, the formulation is general to all discretization methods based on at least C^1 approximations requiring weak enforcement of interface conditions. The proposed methodology can also be easily extended to other flexoelectricity models explicitly accounting for converse flexoelectricity and gradient dielectricity[30,31,32], as well as finite deformations[33,34]. Generalization to other high-order problems is also straightforward.

The paper is organized as follows. Section 2 first briefly describes for completeness the flexoelectricity model and its variational formulation for a body with continuous material properties in an unfitted approach presented in Codony et al.[8], and states next the interface conditions and the variational formulation in the presence of material interfaces, as well as the corresponding weak form. The proposed formulation is then particularized in Section 3 to the weak imposition of generalized periodicity conditions at the fictitious boundaries of periodic unit cells. Section 4 presents the numerical approach for the discretization of the weak form, based on a B-spline approximation with an embedded domain. Numerical experiments in Section 5 demonstrate the applicability and optimal convergence of the proposed technique, including convergence tests with synthetic solutions in 2D and 3D domains with material interfaces, a comb-shaped flexoelectric harvester, and examples of application for the computational modeling of unit cells for flexoelectricity-based metamaterials.

2 | VARIATIONAL FORMULATION FOR COMPOSITE FLEXOELECTRIC MATERIALS

2.1 | Preliminaries

The enthalpy density of a volume $\Omega \in \mathbb{R}^d$, with $d = \{2, 3\}$, of linear flexoelectric material is stated in terms of the displacement $\boldsymbol{u}$ and the electric potential ϕ as [33,35,25,27,8]

$$\mathcal{H}^{\Omega}[\boldsymbol{u}, \phi] = \frac{1}{2}\varepsilon_{ij}\mathbb{C}_{ijkl}\varepsilon_{kl} + \frac{1}{2}\varepsilon_{ij,k}h_{ijklmn}\varepsilon_{lm,n} - \frac{1}{2}E_l\epsilon_{lm}E_m - E_l e_{lij}\varepsilon_{ij} - E_l\mu_{lijk}\varepsilon_{ij,k}, \tag{1}$$

with the strain and the electric field defined as

$$[\boldsymbol{\varepsilon}(\boldsymbol{u})]_{ij} = [\boldsymbol{\varepsilon}(\boldsymbol{u})]_{ji} = \left[\nabla^s(\boldsymbol{u})\right]_{ij} = \frac{1}{2}(u_{i,j} + u_{j,i}), \tag{2}$$

$$[\boldsymbol{E}(\phi)]_l = -[\nabla\phi]_l = -\phi_{,l}, \tag{3}$$

and being $\mathbb{C}_{ijkl}$ the elasticity tensor, h_{ijklmn} the strain-gradient elasticity tensor, ϵ_{lm} the dielectricity tensor, e_{lij} the piezoelectric tensor and μ_{lijk} the flexoelectric tensor. Einstein's summation notation is used, i.e. repeated indices sum over the spatial dimensions. Indexes after a comma denote spatial derivatives; for instance, $u_{i,j} = \partial u_i/\partial x_j$. The work of external loads is

$$\mathcal{W}^{\Omega}[\boldsymbol{u}, \phi] = -b_i u_i + q\phi, \tag{4}$$

where $\mathbf{b}$ are body force and q are free charges. The total bulk enthalpy of a flexoelectric material is then

$$\Pi^{\Omega}[\boldsymbol{u}, \phi] = \int_{\Omega} \left(\mathcal{H}^{\Omega}[\boldsymbol{u}, \phi] + \mathcal{W}^{\Omega}[\boldsymbol{u}, \phi]\right) \mathrm{d}\Omega. \tag{5}$$

Taking also into account the enthalpies associated to the boundary conditions leads to the following functional:

$$\Pi[\boldsymbol{u}, \phi] = \Pi^{\Omega}[\boldsymbol{u}, \phi] + \Pi^{\text{Dirichlet}}[\boldsymbol{u}, \phi] + \Pi^{\text{Neumann}}[\boldsymbol{u}, \phi], \tag{6}$$

where $\Pi^{\text{Dirichlet}}[\boldsymbol{u}, \phi]$ acts on the Dirichlet boundaries and $\Pi^{\text{Neumann}}[\boldsymbol{u}, \phi]$ acts on the Neumann boundaries. The enthalpy associated to Dirichlet boundaries vanishes in body-fitted approaches because the approximation space satisfies the Dirichlet boundary conditions. Otherwise, Dirichlet conditions are imposed in weak sense, here by means of Nitsche's method [10,9]. Following [8], the definition of $\Pi^{\text{Dirichlet}}[\boldsymbol{u}, \phi]$ and $\Pi^{\text{Neumann}}[\boldsymbol{u}, \phi]$ is

$$\begin{aligned}\Pi^{\text{Dirichlet}}[\boldsymbol{u}, \phi] = &\int_{\partial\Omega_u} \left(\frac{1}{2}\beta^u\left(u_i - \bar{u}_i\right)^2 - \left(u_i - \bar{u}_i\right)t_i(\boldsymbol{u}, \phi)\right) \mathrm{d}\Gamma + \int_{\partial\Omega_v} \left(\frac{1}{2}\beta^v\left(\partial^n u_i - \overline{v}_i\right)^2 - \left(\partial^n u_i - \overline{v}_i\right)r_i(\boldsymbol{u}, \phi)\right) \mathrm{d}\Gamma + \\ &+ \int_{\partial\Omega_\phi} \left(-\frac{1}{2}\beta^\phi\left(\phi - \bar{\phi}\right)^2 + \left(\phi - \bar{\phi}\right)w(\boldsymbol{u}, \phi)\right) \mathrm{d}\Gamma + \int_{C_u} \left(\frac{1}{2}\beta^{C_u}\left(u_i - \bar{u}_i\right)^2 - \left(u_i - \bar{u}_i\right)j_i(\boldsymbol{u}, \phi)\right) \mathrm{ds},\end{aligned} \tag{7}$$

$$\Pi^{\text{Neumann}}[\boldsymbol{u}, \phi] = \int_{\partial\Omega_t} -u_i\bar{t}_i \,\mathrm{d}\Gamma + \int_{\partial\Omega_r} -\partial^n u_i\bar{r}_i \,\mathrm{d}\Gamma + \int_{\partial\Omega_w} \phi\bar{w} \,\mathrm{d}\Gamma + \int_{C_j} -u_i\bar{j}_i \,\mathrm{ds}, \tag{8}$$

with the normal derivative operator $\partial^n(A) := \partial A/\partial\mathbf{n}$, and the unitary exterior normal vector $\mathbf{n}$. In Eqs. (7) and (8), $\bar{\boldsymbol{u}}$ is the prescribed displacement on the first order Dirichlet boundary, $\partial\Omega_u$; $\bar{\boldsymbol{t}}$ is the traction on the first order Neumann boundary, $\partial\Omega_t$ with $\partial\Omega = \overline{\partial\Omega}_t \cup \overline{\partial\Omega}_u$, $\partial\Omega$ being the boundary of the domain Ω; $\overline{\boldsymbol{v}}$ is the normal derivative of the displacement $\partial^n\boldsymbol{u}$ on the second order Dirichlet boundary, $\partial\Omega_v$, and $\bar{\boldsymbol{r}}$ is the double traction on the second order Neumann boundary, $\partial\Omega_r$ with $\partial\Omega = \overline{\partial\Omega}_r \cup \overline{\partial\Omega}_v$. The domain boundary is assumed to be composed of smooth surfaces (curves in 2D) that are joined on sharp boundary edges (corners in 2D). C_j denotes the union of the boundary edges that are shared by two surfaces with first order Neumann conditions, i.e. the edges of $\partial\Omega_t$, where a line (punctual in 2D) force $\bar{\boldsymbol{j}}$ is set. C_u denotes the union of all other edges, i.e. those shared by at least one Dirichlet surface, where the value of $\boldsymbol{u}$ is assumed to be that of the adjacent Dirichlet surface, i.e. $\boldsymbol{u} = \bar{\boldsymbol{u}}$ on $C_u \subset \overline{\partial\Omega}_u$. Finally, $\bar{\phi}$ is the prescribed potential on the Dirichlet boundary $\partial\Omega_\phi$, and $\bar{w}$ is the surface charge density on the Neumann boundary $\partial\Omega_w$, with $\partial\Omega = \overline{\partial\Omega}_\phi \cup \overline{\partial\Omega}_w$. Integrals on edges, as the ones on C_u and C_j in Eqs. (7) and (8), reduce to a sum of the values at the corners in 2D.

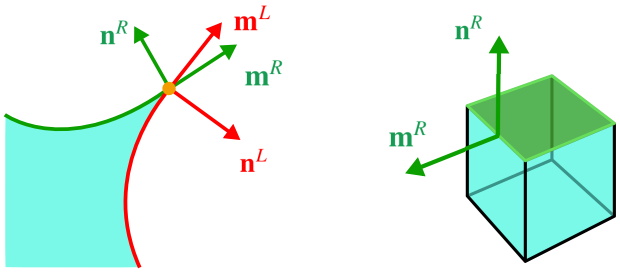

FIGURE 1 Normal vector **n** and conormal vector **m** for 2D and 3D domains, respectively, for the definition (9d) of the forces on C_Ω.

The Nitsche's numerical parameters, β^u, β^v, β^ϕ and β^{C_u}, are positive and large enough to ensure a positive definition of the mechanical problem and a negative definition of the electrical problem, respectively[8]. The traction $t_i(\boldsymbol{u},\phi)$, double traction $r_i(\boldsymbol{u},\phi)$, electric charge density $w(\boldsymbol{u},\phi)$, and edge forces $j_i(\boldsymbol{u},\phi)$ are

$$t_i(\boldsymbol{u},\phi) = \big(\hat{\sigma}_{ij}(\boldsymbol{u},\phi) - \tilde{\sigma}_{ijk,k}(\boldsymbol{u},\phi) - \tilde{\sigma}_{ikj,l}(\boldsymbol{u},\phi)\big(\delta_{lk} - n_l n_k\big)\big)\, n_j + \tilde{\sigma}_{ijk}(\boldsymbol{u},\phi)\tilde{N}_{jk} \quad \text{on } \partial\Omega, \tag{9a}$$

$$r_i(\boldsymbol{u},\phi) = \tilde{\sigma}_{ijk}(\boldsymbol{u},\phi) n_j n_k \quad \text{on } \partial\Omega, \tag{9b}$$

$$w(\boldsymbol{u},\phi) = -\hat{D}_l(\boldsymbol{u},\phi) n_l \quad \text{on } \partial\Omega, \tag{9c}$$

$$j_i(\boldsymbol{u},\phi) = \tilde{\sigma}_{ijk}(\boldsymbol{u},\phi)(m_j^L n_k^L + m_j^R n_k^R) \quad \text{on } C_\Omega, \tag{9d}$$

where $\tilde{N}_{ij} = -n_{i,l}(\delta_{lj} - n_l n_j) + n_{f,g}(\delta_{fg} - n_f n_g) n_i n_j$, $C_\Omega = C_u \cup C_j$ is the set of all edges (corners) of the boundary, the superscripts L and R refer to the first and second surface sharing the edge, and **m** is the conormal vector on each surface, tangent to the surface, normal to the edge and pointing outward to the surface. In 2D, **m** is just the vector tangent to the side and pointing outward on the corner, see Fig. 1.

The stress $\hat{\sigma}_{ij}$, double stress $\tilde{\sigma}_{ijk}$ and electric displacement $\hat{D}_l$ in Eq. (9) are derived from the bulk enthalpy density as

$$\hat{\sigma}_{ij}(\boldsymbol{u},\phi) = \left.\frac{\partial \mathcal{H}^\Omega[\boldsymbol{\varepsilon},\nabla\boldsymbol{\varepsilon},\boldsymbol{E}]}{\partial \varepsilon_{ij}}\right|_{\substack{\nabla\boldsymbol{\varepsilon}\\ \boldsymbol{E}}} = \mathbb{C}_{ijkl}\varepsilon_{kl}(\boldsymbol{u}) - e_{lij}E_l(\phi), \tag{10}$$

$$\tilde{\sigma}_{ijk}(\boldsymbol{u},\phi) = \left.\frac{\partial \mathcal{H}^\Omega[\boldsymbol{\varepsilon},\nabla\boldsymbol{\varepsilon},\boldsymbol{E}]}{\partial \varepsilon_{ij,k}}\right|_{\substack{\boldsymbol{\varepsilon}\\ \boldsymbol{E}}} = h_{ijklmn}\varepsilon_{lm,n}(\boldsymbol{u}) - \mu_{lijk}E_l(\phi), \tag{11}$$

$$\hat{D}_l(\boldsymbol{u},\phi) = -\left.\frac{\partial \mathcal{H}^\Omega[\boldsymbol{\varepsilon},\nabla\boldsymbol{\varepsilon},\boldsymbol{E}]}{\partial E_l}\right|_{\substack{\boldsymbol{\varepsilon}\\ \nabla\boldsymbol{\varepsilon}}} = \epsilon_{lm}E_m(\phi) + e_{lij}\varepsilon_{ij}(\boldsymbol{u}) + \mu_{lijk}\varepsilon_{ij,k}(\boldsymbol{u}). \tag{12}$$

The physical stress is $\sigma_{ij} = \hat{\sigma}_{ij} - \tilde{\sigma}_{ijk,k}$ and the physical electric displacement is $D_i = \hat{D}_i$.

2.2 | Variational formulation in the presence of material interfaces

Let us consider now a physical domain Ω conformed by several non-overlapping subdomains as $\Omega = \bigcup_{i=1}^N \Omega^i$. The boundary of Ω is composed of the exterior boundary, $\partial\overline{\Omega}$, and the interior boundary or interface, $\mathcal{I} = [\bigcup_{i=1}^N \partial\Omega^i]\backslash\partial\overline{\Omega}$, as illustrated in Fig. 2. The interface is split in several parts $\mathcal{I}^k$, each one corresponding to the interface shared by two subdomains, i.e. $\mathcal{I} = \bigcup_{k=1}^{n_f} \mathcal{I}^k$, with $\mathcal{I}^k = \partial\Omega^{L(k)} \cap \partial\Omega^{R(k)}$, being $\Omega^{L(k)}$ and $\Omega^{R(k)}$ the adjacent subdomains. The weighted mean operator and jump operator for a generic function A that may be discontinuous across $\mathcal{I}$, are defined as

$$\{A\}_\gamma = \gamma^{L(k)}A^{L(k)} + \gamma^{R(k)}A^{R(k)}, \qquad [\![A]\!] = A^{L(k)} + A^{R(k)} \quad \text{on} \quad \mathcal{I}^k, \tag{13}$$

with scalar values $\gamma^{L(k)}, \gamma^{R(k)} \in (0,1)$ such that $\gamma^{L(k)} + \gamma^{R(k)} = 1$, and denoting as A^i the value of A in subdomain Ω^i. Although the arithmetic mean is usually enough, ill-conditioning can appear in the presence of cut elements with small area ratio. For that reason, a weighted mean operator is considered. Criteria for the selection of values for γ^L and γ^R are given in Section 4, following a simplified version of parameters reported in Annavarapu et al.[36]. We also define the edges (corners in 2D) of the interface $\mathcal{I}$, which are the boundary of the interfaces except the edges on the Dirichlet boundary, that is $C_\mathcal{I} = \{C^k\}_{k=1}^{n_c} = \bigcup_{f=1}^{n_f} \partial\mathcal{I}^f \backslash C_u$. For

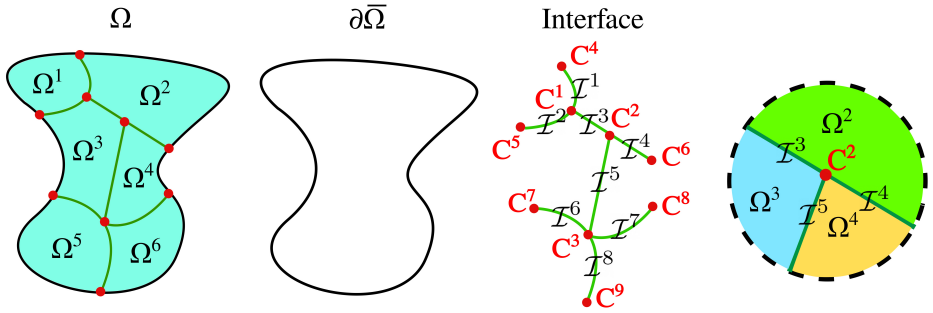

FIGURE 2 Physical domain composed by 6 subdomains with external boundary $\partial\overline{\Omega}$ (in black) and interface $\mathcal{I}$ (in green). An example to illustrate the relative notation around one side and corner is depicted on the right. The interface $\mathcal{I}^3$ is shared by the subdomains $\Omega^{R(3)}$ and $\Omega^{L(3)}$ with $R(3) = 3$ and $L(3) = 2$. The corner C^2 is shared by 3 subdomains $\{\Omega^{P(2,k)}\}_{k=1}^{m(3)}$ with $m(3) = 3$, $P(2,1) = 2$, $P(2,2) = 3$ and $P(2,3) = 4$.

each edge C^k, there are $m(k)$ subdomains $\{\Omega^{P(k,1)}, \Omega^{P(k,2)}, ..., \Omega^{P(k,m(k))}\}$ adjacent to it, see Fig. 2. The weighted mean operator is then also defined on C^k as

$$\langle A \rangle_{\hat{\gamma}} = \sum_{i=1}^{m(k)} \hat{\gamma}^{P(k,i)} A^{P(k,i)} \quad \text{on } C^k \subset C_{\mathcal{I}}, \tag{14}$$

with $\hat{\gamma}^{P(k,i)} \in (0,1)$ such that $\sum_{i=1}^{m(k)} \hat{\gamma}^{P(k,i)} = 1$. It represents a weighted average of the value of A in all the subdomains sharing the edge. The definition of the weighted average in Eq. (14) is a generalization of the one in Eq. (13). Criteria for the selection of $\hat{\gamma}$ are also given in Section 4.

The interface conditions that must be fulfilled at the interface and edges (corners in 2D) enforce continuity of the solution and equilibrium. That is,

$$\left[\!\left[\boldsymbol{u} \otimes \mathbf{n} \right]\!\right] = \mathbf{0}, \quad \left[\!\left[\partial^n \boldsymbol{u} \right]\!\right] = \mathbf{0}, \quad \left[\!\left[\phi \mathbf{n} \right]\!\right] = \mathbf{0}, \quad \left[\!\left[\boldsymbol{t}(\boldsymbol{u}, \phi) \right]\!\right] = \hat{\boldsymbol{t}}, \quad \left[\!\left[\boldsymbol{r}(\boldsymbol{u}, \phi) \otimes \mathbf{n} \right]\!\right] = \hat{\boldsymbol{r}} \otimes \mathbf{n}^L, \quad \left[\!\left[w(\boldsymbol{u}, \phi) \right]\!\right] = \hat{w} \quad \text{on } \mathcal{I}, \tag{15}$$

and

$$\boldsymbol{u}^{P(k,i)} - \langle \boldsymbol{u} \rangle_{\hat{\gamma}} = \mathbf{0} \quad i = 1 \ldots m(k), \qquad \sum_{i=1}^{m(k)} \boldsymbol{j}^{P(k,i)}(\boldsymbol{u}, \phi) = \hat{\boldsymbol{j}} \quad \text{on } C^k \subset C_{\mathcal{I}} \tag{16}$$

where $\boldsymbol{j}^{\alpha}(\boldsymbol{u}, \phi)$ denotes the line force on the edge (punctual force at corners in 2D) coming from the subdomain Ω^{α} sharing the edge. The data is $\hat{\boldsymbol{j}} = \bar{\boldsymbol{j}}$ on edges on the boundary, and $\hat{\boldsymbol{j}} = \mathbf{0}$ on edges in the interior of the domain. Thus, Eq. (16) enforces that the sum of the forces from each subdomain sharing an edge C^k is in internal equilibrium or in equilibrium with external boundary forces. The values of $\hat{\boldsymbol{t}}$, $\hat{\boldsymbol{r}}$ and $\hat{w}$ in Eq. (15) are also zero for physical problems and conveniently set for synthetic solutions.

The enthalpy associated to Eqs. (15) and (16) is analogous to that of Dirichlet boundary conditions, Eq. (7), and Neumann boundary conditions, Eq. (8) Thus, the total enthalpy associated to interfaces is

$$\begin{aligned}
\Pi^{\text{Interface}}[\boldsymbol{u}, \phi] = &\int_{\mathcal{I}} \left[\frac{1}{2} \beta^{u\mathcal{I}} \left[\!\left[u_i n_j \right]\!\right]^2 - \left[\!\left[u_i n_j \right]\!\right] \left\{ t_i(\boldsymbol{u}, \phi) n_j \right\}_{\gamma} - \hat{t}_i \left\{ u_i \right\}_{1-\gamma} \right] \mathrm{d}\Gamma + \\
&+ \int_{\mathcal{I}} \left[\frac{1}{2} \beta^{v\mathcal{I}} \left[\!\left[\partial^n u_i \right]\!\right]^2 - \left[\!\left[\partial^n u_i \right]\!\right] \left\{ r_i(\boldsymbol{u}, \phi) \right\}_{\gamma} - \hat{r}_i n_j^L \left\{ u_{i,j} \right\}_{1-\gamma} \right] \mathrm{d}\Gamma + \\
&+ \int_{\mathcal{I}} \left[-\frac{1}{2} \beta^{\phi\mathcal{I}} \left[\!\left[\phi n_i \right]\!\right]^2 + \left[\!\left[\phi n_i \right]\!\right] \left\{ w(\boldsymbol{u}, \phi) n_i \right\}_{\gamma} + \hat{w} \left\{ \phi \right\}_{1-\gamma} \right] \mathrm{d}\Gamma + \\
&+ \sum_{k=1}^{n_C} \int_{C^k} \left[\sum_{\alpha \in P(k,:)} \left(\frac{1}{2} \beta^{C_u \mathcal{I}} (u_i^{\alpha} - \langle u_i \rangle_{\hat{\gamma}})^2 - (u_i^{\alpha} - \langle u_i \rangle_{\hat{\gamma}}) j_i^{\alpha}(\boldsymbol{u}, \phi) \right) - \langle u_i \rangle_{\hat{\gamma}} \hat{j}_i \right] \mathrm{ds}.
\end{aligned} \tag{17}$$

where $P(k,:) = \{P(k,1), ..., P(k,m(k))\}$.

The penalty parameters $\beta^{u\mathcal{I}}$, $\beta^{v\mathcal{I}}$, $\beta^{\phi\mathcal{I}}$ and $\beta^{C_u\mathcal{I}}$ in Eq. (17) must be large enough to ensure concave up enthalpy with respect to the displacement $\boldsymbol{u}$, and concave down enthalpy with respect to the electric potential ϕ. Practical lower bounds and the scaling with the mesh size and material parameters are commented in Section 4.

The total enthalpy of the domain Ω with material interfaces is then

$$\Pi[\boldsymbol{u},\phi] = \Pi^{\Omega}[\boldsymbol{u},\phi] + \Pi^{\text{Dirichlet}}[\boldsymbol{u},\phi] + \Pi^{\text{Neumann}}[\boldsymbol{u},\phi] + \Pi^{\text{Interface}}[\boldsymbol{u},\phi]. \tag{18}$$

The variational principle is

$$(\boldsymbol{u}^*,\phi^*) = \arg\min_{\boldsymbol{u}\in\mathcal{U}} \max_{\phi\in\mathcal{H}^1(\Omega)} \Pi[\boldsymbol{u},\phi], \tag{19}$$

where $\mathcal{U}$ is the space of functions belonging to $[\mathcal{H}^2(\Omega)]^d$ with $\mathcal{L}^2$-integrable third derivative on the Dirichlet boundary $\partial\Omega_u$.

2.3 | Weak form of the boundary value problem

The weak form of the problem is derived from the first-order stationarity condition

$$\delta\Pi[\boldsymbol{u},\phi;\delta\boldsymbol{u},\delta\phi] = 0, \quad \forall\delta\boldsymbol{u}\in\mathcal{U},\ \delta\phi\in\mathcal{H}^1(\Omega), \tag{20}$$

where

$$\delta\Pi[\boldsymbol{u},\phi;\delta\boldsymbol{u},\delta\phi] = \delta\Pi^{\Omega}[\boldsymbol{u},\phi;\delta\boldsymbol{u},\delta\phi] + \delta\Pi^{\text{Dirichlet}}[\boldsymbol{u},\phi;\delta\boldsymbol{u},\delta\phi] + \delta\Pi^{\text{Neumann}}[\delta\boldsymbol{u},\delta\phi] + \delta\Pi^{\text{Interface}}[\boldsymbol{u},\phi;\delta\boldsymbol{u},\delta\phi], \tag{21}$$

with

$$\delta\Pi^{\Omega}[\boldsymbol{u},\phi;\delta\boldsymbol{u},\delta\phi] = \int_{\Omega} \left(\hat{\sigma}_{ij}(\boldsymbol{u},\phi)\varepsilon_{ij}(\delta\boldsymbol{u}) + \tilde{\sigma}_{ijk}(\boldsymbol{u},\phi)\varepsilon_{ij,k}(\delta\boldsymbol{u}) - \hat{D}_l(\boldsymbol{u},\phi)E_l(\delta\phi) - b_i\delta u_i + q\delta\phi\right)\mathrm{d}\Omega, \tag{22}$$

$$\begin{aligned}\delta\Pi^{\text{Dirichlet}}[\boldsymbol{u},\phi;\delta\boldsymbol{u},\delta\phi] = &\int_{\partial\Omega_u} \left(\beta^u\left(u_i-\bar{u}_i\right)\delta u_i - t_i(\boldsymbol{u},\phi)\delta u_i - \left(u_i-\bar{u}_i\right)t_i(\delta\boldsymbol{u},\delta\phi)\right)\mathrm{d}\Gamma + \\ &+\int_{\partial\Omega_v} \left(\beta^v\left(\partial^n u_i-\overline{v}_i\right)\partial^n\delta u_i - r_i(\boldsymbol{u},\phi)\partial^n\delta u_i - \left(\partial^n u_i-\overline{v}_i\right)r_i(\delta\boldsymbol{u},\delta\phi)\right)\mathrm{d}\Gamma + \\ &+\int_{\partial\Omega_\phi} \left(-\beta^\phi\left(\phi-\bar{\phi}\right)\delta\phi + w(\boldsymbol{u},\phi)\delta\phi + \left(\phi-\bar{\phi}\right)w(\delta\boldsymbol{u},\delta\phi)\right)\mathrm{d}\Gamma + \\ &+\int_{C_u} \left(\beta^{C_u}\left(u_i-\bar{u}_i\right)\delta u_i - j_i(\boldsymbol{u},\phi)\delta u_i - \left(u_i-\bar{u}_i\right)j_i(\delta\boldsymbol{u},\delta\phi)\right)\mathrm{ds},\end{aligned} \tag{23}$$

$$\delta\Pi^{\text{Neumann}}[\delta\boldsymbol{u},\delta\phi] = \int_{\partial\Omega_t} -\bar{t}_i\delta u_i\,\mathrm{d}\Gamma + \int_{\partial\Omega_r} -\bar{r}_i\partial^n\delta u_i\,\mathrm{d}\Gamma + \int_{\partial\Omega_w} \bar{w}\delta\phi\,\mathrm{d}\Gamma \int_{C_j} -\bar{j}_i\delta u_i\,\mathrm{ds}, \tag{24}$$

$$\delta\Pi^{\text{Interface}}[\boldsymbol{u},\phi,\delta\boldsymbol{u},\delta\phi] = \int_{\mathcal{I}} \left[\beta^{u\mathcal{I}} \left[\!\left[\delta u_i n_j\right]\!\right] \left[\!\left[u_i n_j\right]\!\right] - \left[\!\left[\delta u_i n_j\right]\!\right] \left\{ t_i(\boldsymbol{u},\phi) n_j \right\}_\gamma - \left[\!\left[u_i n_j\right]\!\right] \left\{ t_i(\delta\boldsymbol{u},\delta\phi) n_j \right\}_\gamma - \hat{t}_i \left\{ \delta u_i \right\}_{1-\gamma} \right] \mathrm{d}\Gamma +$$
$$+ \int_{\mathcal{I}} \left[\beta^{v\mathcal{I}} \left[\!\left[\partial^n \delta u_i\right]\!\right] \left[\!\left[\partial^n u_i\right]\!\right] - \left[\!\left[\partial^n \delta u_i\right]\!\right] \left\{ r_i(\boldsymbol{u},\phi) \right\}_\gamma - \left[\!\left[\partial^n u_i\right]\!\right] \left\{ r_i(\delta\boldsymbol{u},\delta\phi) \right\}_\gamma - \hat{r}_i n_j^L \left\{ \delta u_{i,j} \right\}_{1-\gamma} \right] \mathrm{d}\Gamma +$$
$$+ \int_{\mathcal{I}} \left[-\beta^{\phi\mathcal{I}} \left[\!\left[\delta\phi n_i\right]\!\right] \left[\!\left[\phi n_i\right]\!\right] + \left[\!\left[\delta\phi n_i\right]\!\right] \left\{ w(\boldsymbol{u},\phi) n_i \right\}_\gamma + \left[\!\left[\phi n_i\right]\!\right] \left\{ w(\delta\boldsymbol{u},\delta\phi) n_j \right\}_\gamma + i\hat{w} \left\{ \delta\phi \right\}_{1-\gamma} \right] \mathrm{d}\Gamma +$$
$$+ \sum_{k=1}^{n_C} \int_{C^k} \left[\sum_{\alpha\in P(k,:)} \left(\beta^{C_u\mathcal{I}} \left(u_i^\alpha - \langle u_i\rangle_{\hat{\gamma}}\right)\left(\delta u_i^\alpha - \langle \delta u_i\rangle_{\hat{\gamma}}\right) - \left(u_i^\alpha - \langle u_i\rangle_{\hat{\gamma}}\right) j_i^\alpha(\delta\boldsymbol{u},\delta\phi) - \right.\right.$$
$$\left.\left. - j_i^\alpha(\boldsymbol{u},\phi)\delta u_i^\alpha \right) \mathrm{d}\Gamma - \hat{\gamma}^\alpha \left(\hat{j}_i - \sum_{\tau\in P(k;:)} j_i^\tau(\boldsymbol{u},\phi)\right)\delta u_i^\alpha \Bigg) \Bigg] \mathrm{d}s. \tag{25}$$

In addition, the following conditions ensure a well-posed saddle point problem:

$$\delta_u^2\Pi[\boldsymbol{u},\phi;\delta\boldsymbol{u}] > 0, \quad \delta_\phi^2\Pi[\boldsymbol{u},\phi;\delta\phi] < 0, \quad \forall\delta\boldsymbol{u},\delta\phi. \tag{26}$$

Finally, the weak form of the problem is

$$\textit{Find } (\boldsymbol{u},\phi) \in \mathcal{U} \otimes \mathcal{H}^1(\Omega) \textit{ such that } \delta\Pi[\boldsymbol{u},\phi;\delta\boldsymbol{u},\delta\phi] = 0, \forall(\delta\boldsymbol{u},\delta\phi) \in \mathcal{U} \otimes \mathcal{H}^1(\Omega). \tag{27}$$

3 | VARIATIONAL FORMULATION FOR GENERALIZED PERIODIC UNIT CELLS

Periodic structures are obtained by periodically replicating a structural unit cell in 1, 2 or 3 spatial dimensions. Boundary value problems on periodic structures can be efficiently solved by reducing them to the unit cell with so-called generalized periodic conditions in the direction of periodicity[37,38]. These conditions aim at replicating the macroscopic loading conditions of a unit cell in an infinitely periodic structure, and are thus devoid of sample's finite-size effects. These macroscopic loading conditions can be mapped to jumps of the primary variables $\boldsymbol{u}$ and ϕ between the unit cell fictitious periodic boundaries. Since flexoelectricity governing equations are a system of 4th-order PDEs, generalized periodicity needs to be supplemented with appropriate periodicity conditions for the high-order fields, enforcing C^1 continuity of the primary fields. In unfitted discretizations, high-order generalized periodicity conditions can be enforced weakly using the formalism for physical interfaces presented in Section 2, as described next.

3.1 | Generalized periodicity conditions

For the sake of simplicity, let us restrict ourselves to a 2D lattice that is periodically replicated along $x-$ and $y-$ spatial directions. The unit cell Ω is embedded in a rectangle $R = [0, L_x] \times [0, L_y]$, as shown in the example in Fig. 3. The boundary of the domain Ω is composed of generalized periodic boundaries, $\mathcal{I}^y = \{(x,0) \in \partial\Omega\} \equiv \{(x, L_y) \in \partial\Omega\}$ and $\mathcal{I}^x = \{(0,y) \in \partial\Omega\} \equiv \{(L_x, y) \in \partial\Omega\}$, and physical boundaries in the interior of the rectangle, $\partial\Omega\backslash[\mathcal{I}^x \cup \mathcal{I}^y]$.

We define C^x as the set of values of y-component of the corners in $\mathcal{I}^x$ and C^y as the set of values of x-component of the corners in $\mathcal{I}^y$, see Fig. 3. The generalized periodicity conditions of the unit cell are then

$$\begin{array}{llll}
\left[\!\left[\boldsymbol{u}\right]\!\right]^y = \breve{\boldsymbol{u}}^y, & \left[\!\left[\dfrac{\partial\boldsymbol{u}}{\partial y}\right]\!\right]^y = \boldsymbol{0}, & \left[\!\left[\phi\right]\!\right]^y = \breve{\phi}^y, & \\
\boldsymbol{t}(\boldsymbol{u},\phi)|_{y=L_y} + \boldsymbol{t}(\boldsymbol{u},\phi)|_{y=0} = \boldsymbol{0}, & \left[\!\left[\boldsymbol{r}(\boldsymbol{u},\phi)\right]\!\right]^y = \boldsymbol{0}, & w(\boldsymbol{u},\phi)|_{y=L_y} + w(\boldsymbol{u},\phi)|_{y=0} = \boldsymbol{0} & \text{on } \mathcal{I}^y, \\
\left[\!\left[\boldsymbol{u}\right]\!\right]^y = \breve{\boldsymbol{u}}^y, & & \boldsymbol{j}(\boldsymbol{u},\phi)|_{y=L_y} + \boldsymbol{j}(\boldsymbol{u},\phi)|_{y=0} = \boldsymbol{0} & \text{for } x \in C^y, \\
\left[\!\left[\boldsymbol{u}\right]\!\right]^x = \breve{\boldsymbol{u}}^x, & \left[\!\left[\dfrac{\partial\boldsymbol{u}}{\partial x}\right]\!\right]^x = \boldsymbol{0}, & \left[\!\left[\phi\right]\!\right]^x = \breve{\phi}^x, & \\
\boldsymbol{t}(\boldsymbol{u},\phi)|_{x=L_x} + \boldsymbol{t}(\boldsymbol{u},\phi)|_{x=0} = \boldsymbol{0}, & \left[\!\left[\boldsymbol{r}(\boldsymbol{u},\phi)\right]\!\right]^x = \boldsymbol{0}, & w(\boldsymbol{u},\phi)|_{x=L_x} + w(\boldsymbol{u},\phi)|_{x=0} = \boldsymbol{0} & \text{on } \mathcal{I}^x, \\
\left[\!\left[\boldsymbol{u}\right]\!\right]^x = \breve{\boldsymbol{u}}^x, & & \boldsymbol{j}(\boldsymbol{u},\phi)|_{x=L_x} + \boldsymbol{j}(\boldsymbol{u},\phi)|_{x=0} = \boldsymbol{0} & \text{for } y \in C^x,
\end{array} \tag{28}$$

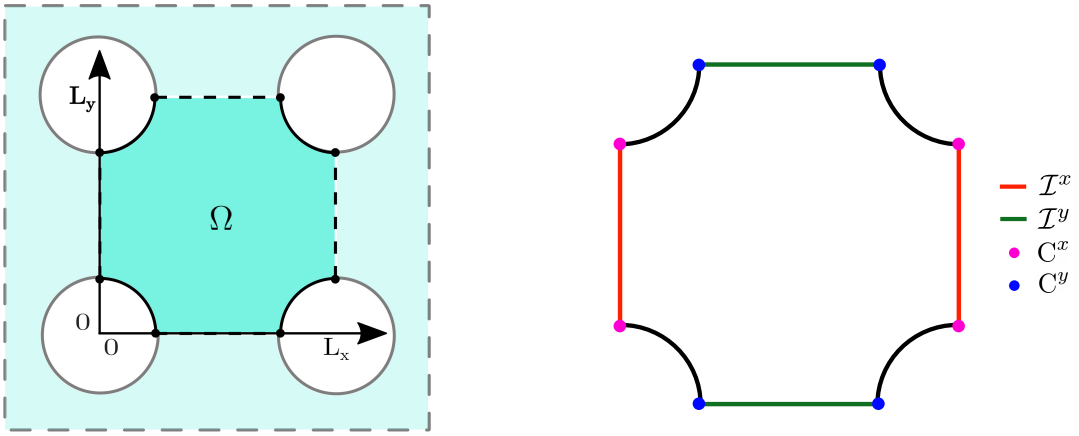

FIGURE 3 Example of one unit cell of a periodic structure, $C^x = \{L_y/4, 3L_y/4\}$ and $C^y = \{L_x/4, 3L_x/4\}$.

where the jump on the periodic boundaries is defined as

$$[\![A]\!]^y = A(x, L_y) - A(x, 0), \quad [\![A]\!]^x = A(L_x, y) - A(0, y), \tag{29}$$

for convenience. The jumps $\check{\boldsymbol{u}}^y$, $\check{\boldsymbol{u}}^x$, $\check{\phi}^y$ and $\check{\phi}^x$ can be either given constants (mapped from the applied load at the macroscopic level) or unknown constants that have to be determined assuming a prescribed value of their macroscopic work-conjugate (generally – but not necessarily – null). For the case of a vertical displacement sensor, where a vertical macroscopic strain is applied, $\check{\boldsymbol{u}}^y = (0, \check{u}^y)$, with $\check{u}^y$ a known constant, and the displacement jump $\check{\boldsymbol{u}}^x$, and electric potential jumps, $\check{\phi}^y$ and $\check{\phi}^x$, are unknowns to be computed assuming vanishing macrotractions on the vertical unit cell boundaries and that no surface charges accumulate on unit cell boundaries, i.e. $\boldsymbol{D} \cdot \mathbf{n} = 0$ on $\mathcal{I}^x$ and $\mathcal{I}^y$,$\boldsymbol{D}$ being the macroscopic physical electric displacement[39]. Other boundary value problems on the generalized periodic unit cell can also be defined analogously. For instance, for the case of a displacement actuator, an electric potential difference is applied macroscopically, which can be mapped to known electric potential jumps in the unit cell, $\check{\phi}^y$ and $\check{\phi}^x$, and the unknown displacement jumps $\check{\boldsymbol{u}}^y$ and $\check{\boldsymbol{u}}^x$, are then computed assuming that the unit cell is unconfined[39].

Remark 1. Generalized periodicity conditions at the corners of R. If the corners of the rectangle lie inside the material domain, then generalized periodicity conditions for both $\mathcal{I}_x$ and $\mathcal{I}_y$ must be enforced simultaneously. For instance, the definition in Eq. (29) becomes

$$[\![A]\!]^y = A(L_x, L_y) - A(L_x, 0) + A(0, L_y) - A(0, 0), \quad [\![A]\!]^x = A(L_x, L_y) - A(0, L_y) + A(L_x, 0) - A(0, 0), \tag{30}$$

at the vertex. This situation can be avoided in general by a suitable choice of unit cell.

The total enthalpy of the system is

$$\Pi[\boldsymbol{u}, \phi, \check{\boldsymbol{u}}, \check{\phi}] = \Pi^{\Omega}[\boldsymbol{u}, \phi] + \Pi^{\text{Dirichlet}}[\boldsymbol{u}, \phi] + \Pi^{\text{Neumann}}[\boldsymbol{u}, \phi] + \Pi^{\text{P,y}}[\boldsymbol{u}, \phi, \check{\boldsymbol{u}}, \check{\phi}] + \Pi^{\text{P,x}}[\boldsymbol{u}, \phi, \check{\boldsymbol{u}}, \check{\phi}], \tag{31}$$

with Eqs. (5), (7), (8) and the enthalpy associated to periodic boundaries

$$\begin{aligned}
\Pi^{\text{P,y}}[\boldsymbol{u}, \phi, \check{\boldsymbol{u}}, \check{\phi}] = & \int_{\mathcal{I}^y} \left[\frac{1}{2} \beta^{uy} \Big([\![u_i]\!]^y - \check{u}_i^y \Big)^2 - \Big([\![u_i]\!]^y - \check{u}_i^y \Big) [\![t_i(\boldsymbol{u}, \phi)]\!]_\gamma^y \right] \mathrm{d}\Gamma \\
& + \int_{\mathcal{I}^y} \left[\frac{1}{2} \beta^{vy} \Big(\left[\!\!\left[\frac{\partial u_i}{\partial y} \right]\!\!\right]^y \Big)^2 - \left[\!\!\left[\frac{\partial u_i}{\partial y} \right]\!\!\right]^y \Big\{ r_i(\boldsymbol{u}, \phi) \Big\}_\gamma^y \right] \mathrm{d}\Gamma + \\
& + \int_{\mathcal{I}^y} \left[-\frac{1}{2} \beta^{\phi y} \Big([\![\phi]\!]^y - \check{\phi}^y \Big)^2 + \Big([\![\phi]\!]^y - \check{\phi}^y \Big) [\![w(\boldsymbol{u}, \phi)]\!]_\gamma^y \right] \mathrm{d}\Gamma + \\
& + \sum_{x \in C^y} \left[\frac{1}{2} \beta^{C_u y} \Big([\![u_i]\!]^y - \check{u}_i^y \Big)^2 - \Big([\![u_i]\!]^y - \check{u}_i^y \Big) [\![j_i(\boldsymbol{u}, \phi)]\!]_\gamma^y \right],
\end{aligned} \tag{32}$$

$$\Pi^{\mathrm{P,x}}[\boldsymbol{u},\phi,\breve{\boldsymbol{u}},\breve{\phi}] = \int_{I^x}\left[\frac{1}{2}\beta^{ux}\Big(\llbracket u_i\rrbracket^x-\breve{u}_i^x\Big)^2-\Big(\llbracket u_i\rrbracket^x-\breve{u}_i^x\Big)\llbracket t_i(\boldsymbol{u},\phi)\rrbracket_\gamma^x\right]\mathrm{d}\Gamma$$
$$+\int_{I^x}\left[\frac{1}{2}\beta^{vx}\Big(\left\llbracket\frac{\partial u_i}{\partial x}\right\rrbracket^x\Big)^2-\left\llbracket\frac{\partial u_i}{\partial x}\right\rrbracket^x\Big\{r_i(\boldsymbol{u},\phi)\Big\}_\gamma^x\right]\mathrm{d}\Gamma+$$
$$+\int_{I^x}\left[-\frac{1}{2}\beta^{\phi x}\Big(\llbracket\phi\rrbracket^x-\breve{\phi}^x\Big)^2+\Big(\llbracket\phi\rrbracket^x-\breve{\phi}^x\Big)\llbracket w(\boldsymbol{u},\phi)\rrbracket_\gamma^x\right]\mathrm{d}\Gamma+$$
$$+\sum_{y\in C^x}\left[\frac{1}{2}\beta^{C_u x}\Big(\llbracket u_i\rrbracket^x-\breve{u}_i^x\Big)^2-\Big(\llbracket u_i\rrbracket^x-\breve{u}_i^x\Big)\llbracket j_i(\boldsymbol{u},\phi)\rrbracket_\gamma^x\right], \tag{33}$$

where $\breve{\boldsymbol{u}}=\{\breve{\boldsymbol{u}}^x,\breve{\boldsymbol{u}}^y\}$, $\breve{\phi}=\{\breve{\phi}^x,\breve{\phi}^y\}$ and the weighted means and jumps on the periodic boundaries are defined as

$$\{A\}_\gamma^y=\gamma A(x,L_y)+(1-\gamma)A(x,0) \qquad \{A\}_\gamma^x=\gamma A(L_x,y)+(1-\gamma)A(0,y)$$
$$\llbracket A\rrbracket_\gamma^y=\gamma A(x,L_y)-(1-\gamma)A(x,0) \qquad \llbracket A\rrbracket_\gamma^x=\gamma A(L_x,y)-(1-\gamma)A(0,y) \tag{34}$$

with $\gamma\in(0,1)$.

In Eqs. (32) and (33), it is important to distinguish the cases where the jumps $\breve{\boldsymbol{u}}^{(\cdot)}$ or $\breve{\phi}^{(\cdot)}$ are prescribed or unknown. For prescribed values of $\breve{\boldsymbol{u}}^{(\cdot)}$ or $\breve{\phi}^{(\cdot)}$, we directly substitute $\breve{\boldsymbol{u}}^{(\cdot)}$ or $\breve{\phi}^{(\cdot)}$ by its prescribed value $\hat{\boldsymbol{u}}^{(\cdot)}$ or $\hat{\phi}^{(\cdot)}$ so that Eqs. (32) and (33) are analogous to Eq. (25). For unknown values of $\breve{\boldsymbol{u}}^{(\cdot)}$ or $\breve{\phi}^{(\cdot)}$, Eqs. (32) and (33) weakly enforce a constraint between state variables, and therefore do not admit penalty terms, i.e. the corresponding $\beta^{(\cdot)}$ must be set to zero.

3.2 | Variational formulation and weak form

For the sake of simplicity, we restrict now to the case of a vertical displacement sensor, where a uniform vertical strain is applied at the macroscopic level, allowing free macroscopic transversal deformation of the material, and assuming that no surface charges accumulate macroscopically. This case is considered in the example in Section 5.4. The particularization to other generalized periodic boundary value problems is straightforward.

The condition to be imposed weakly is $\breve{\boldsymbol{u}}^y=\hat{\boldsymbol{u}}^y$, with a prescribed vertical displacement jump $\hat{\boldsymbol{u}}^y$ mapped from the applied vertical macroscopic strain. The horizontal jump of the displacement $\breve{\boldsymbol{u}}^x$ and the electric potential jump $\breve{\phi}$ are unknown constants. Hence, in Eqs. (32) and (33), the penalty parameters β^{ux}, $\beta^{C_u x}$, $\beta^{\phi x}$ and $\beta^{\phi y}$ must be set to 0, and $\breve{\boldsymbol{u}}^y=\hat{\boldsymbol{u}}^y$. The solution of the associated boundary value problem then follows from the variational principle

$$(\boldsymbol{u}^*,\phi^*,\breve{\boldsymbol{u}}^{x*},\breve{\phi}^*)=\arg\min_{\boldsymbol{u}\in\mathcal{U}}\max_{\phi\in\mathcal{H}^1(\Omega)}\max_{\breve{\boldsymbol{u}}^x\in\mathbb{R}^2}\min_{\breve{\phi}\in\mathbb{R}^2}\Pi[\boldsymbol{u},\phi,\breve{\boldsymbol{u}}^x,\breve{\phi}]. \tag{35}$$

The weak form of the problem follows from stationarity of the enthalpy functional in Eq. (31)

$$\delta\Pi[\boldsymbol{u},\phi,\breve{\boldsymbol{u}}^x,\breve{\phi};\delta\boldsymbol{u},\delta\phi,\delta\breve{\boldsymbol{u}}^x,\delta\breve{\phi}]=0;\quad\forall\delta\boldsymbol{u},\delta\phi,\delta\breve{\boldsymbol{u}}^x,\delta\breve{\phi}, \tag{36}$$

together with the second order stationarity conditions

$$\delta^2_{\boldsymbol{u}}\Pi[\boldsymbol{u},\phi,\breve{\boldsymbol{u}}^x,\breve{\phi};\delta\boldsymbol{u}]>0, \qquad \delta^2_{\phi}\Pi[\boldsymbol{u},\phi,\breve{\boldsymbol{u}}^x,\breve{\phi};\delta\phi]<0,$$
$$\delta^2_{\breve{\boldsymbol{u}}^x}\Pi[\boldsymbol{u},\phi,\breve{\boldsymbol{u}}^x,\breve{\phi};\delta\breve{\boldsymbol{u}}^x]<0, \qquad \delta^2_{\breve{\phi}}\Pi[\boldsymbol{u},\phi,\breve{\boldsymbol{u}}^x,\breve{\phi};\delta\breve{\phi}]>0, \tag{37}$$

where

$$\delta\Pi[\boldsymbol{u},\phi,\breve{\boldsymbol{u}}^x,\breve{\phi};\delta\boldsymbol{u},\delta\phi,\delta\breve{\boldsymbol{u}}^x,\delta\breve{\phi}]=\delta\Pi^{\Omega}[\boldsymbol{u},\phi;\delta\boldsymbol{u},\delta\phi]+\delta\Pi^{\mathrm{Dirichlet}}[\boldsymbol{u},\phi;\delta\boldsymbol{u},\delta\phi]+\delta\Pi^{\mathrm{Neumann}}[\delta\boldsymbol{u},\delta\phi]$$
$$+\delta\Pi^{\mathrm{P,y}}[\boldsymbol{u},\phi,\breve{\boldsymbol{u}}^x,\breve{\phi};\delta\boldsymbol{u},\delta\phi,\delta\breve{\boldsymbol{u}}^x,\delta\breve{\phi}]+\delta\Pi^{\mathrm{P,x}}[\boldsymbol{u},\phi,\breve{\boldsymbol{u}}^x,\breve{\phi};\delta\boldsymbol{u},\delta\phi,\delta\breve{\boldsymbol{u}}^x,\delta\breve{\phi}], \tag{38}$$

$\delta\Pi^{\Omega}$, $\delta\Pi^{\mathrm{Dirichlet}}$ and $\delta\Pi^{\mathrm{Neumann}}$ are defined in Eqs. (22), (23) and (24), and

$$
\begin{aligned}
&\delta\Pi^{\mathrm{P,y}}[\boldsymbol{u},\phi,\breve{\boldsymbol{u}}^x,\breve{\phi};\delta\boldsymbol{u},\delta\phi,\delta\breve{\boldsymbol{u}}^x,\delta\breve{\phi}] = \\
&\int_{\mathcal{I}^y}\left[\beta^{uy}\,[\![\delta u_i]\!]^y\left([\![u_i]\!]^y-\hat{u}_i^y\right)-[\![\delta u_i]\!]^y\,[\![t_i(\boldsymbol{u},\phi)]\!]_\gamma^y-\left([\![u_i]\!]^y-\hat{u}_i^y\right)[\![t_i(\delta\boldsymbol{u},\delta\phi)]\!]_\gamma^y\right]\mathrm{d}\Gamma \\
&+\int_{\mathcal{I}^y}\left[\beta^{vy}\left[\!\left[\frac{\partial u_i}{\partial y}\right]\!\right]^y\left[\!\left[\frac{\partial\delta u_i}{\partial y}\right]\!\right]^y-\left[\!\left[\frac{\partial\delta u_i}{\partial y}\right]\!\right]^y\left\{r_i(\boldsymbol{u},\phi)\right\}_\gamma^y-\left[\!\left[\frac{\partial u_i}{\partial y}\right]\!\right]^y\left\{r_i(\delta\boldsymbol{u},\delta\phi)\right\}_\gamma^y\right]\mathrm{d}\Gamma+ \\
&+\int_{\mathcal{I}^y}\left[\left([\![\delta\phi]\!]^y-\delta\breve{\phi}^y\right)[\![w(\boldsymbol{u},\phi)]\!]_\gamma^y+\left([\![\phi]\!]^y-\breve{\phi}^y\right)[\![w(\delta\boldsymbol{u},\delta\phi)]\!]_\gamma^y\right]\mathrm{d}\Gamma \\
&+\sum_{x\in C^y}\left[\beta^{C_u y}\,[\![\delta u_i]\!]^y\left([\![u_i]\!]^y-\hat{u}_i^y\right)-[\![\delta u_i]\!]^y\,[\![j_i(\boldsymbol{u},\phi)]\!]_\gamma^y-\left([\![u_i]\!]^y-\hat{u}_i^y\right)[\![j_i(\delta\boldsymbol{u},\delta\phi)]\!]_\gamma^y\right],
\end{aligned}
\tag{39}
$$

$$
\begin{aligned}
&\delta\Pi^{\mathrm{P,x}}[\boldsymbol{u},\phi,\breve{\boldsymbol{u}}^x,\breve{\phi};\delta\boldsymbol{u},\delta\phi,\delta\breve{\boldsymbol{u}}^x,\delta\breve{\phi}] = \\
&\int_{\mathcal{I}^x}\left[-\left([\![\delta u_i]\!]^x-\delta\breve{u}_i^x\right)[\![t_i(\boldsymbol{u},\phi)]\!]_\gamma^x-\left([\![u_i]\!]^x-\breve{u}_i^x\right)[\![t_i(\delta\boldsymbol{u},\delta\phi)]\!]_\gamma^x\right]\mathrm{d}\Gamma \\
&+\int_{\mathcal{I}^x}\left[\beta^{vx}\left[\!\left[\frac{\partial u_i}{\partial x}\right]\!\right]^x\left[\!\left[\frac{\partial\delta u_i}{\partial x}\right]\!\right]^x-\left[\!\left[\frac{\partial\delta u_i}{\partial x}\right]\!\right]^x\left\{r_i(\boldsymbol{u},\phi)\right\}_\gamma^x-\left[\!\left[\frac{\partial u_i}{\partial x}\right]\!\right]^x\left\{r_i(\delta\boldsymbol{u},\delta\phi)\right\}_\gamma^x\right]\mathrm{d}\Gamma+ \\
&+\int_{\mathcal{I}^x}\left[\left([\![\delta\phi]\!]^x-\delta\breve{\phi}^x\right)[\![w(\boldsymbol{u},\phi)]\!]_\gamma^x+\left([\![\phi]\!]^x-\breve{\phi}^x\right)[\![w(\delta\boldsymbol{u},\delta\phi)]\!]_\gamma^x\right]\mathrm{d}\Gamma \\
&+\sum_{y\in C^x}\left[-\left([\![\delta u_i]\!]^x-\delta\breve{u}_i^x\right)[\![j_i(\boldsymbol{u},\phi)]\!]_\gamma^x-\left([\![u_i]\!]^x-\breve{u}_i^x\right)[\![j_i(\delta\boldsymbol{u},\delta\phi)]\!]_\gamma^x\right],
\end{aligned}
\tag{40}
$$

being $\delta\breve{\boldsymbol{u}}$ and $\delta\breve{\phi}$ admissible variations of $\breve{\boldsymbol{u}}$ and $\breve{\phi}$, respectively. Finally the weak form associated to the boundary value problem reads

$$
\textit{Find } (\boldsymbol{u},\phi,\breve{\boldsymbol{u}}^x,\breve{\phi})\in\mathcal{U}\otimes\mathcal{H}^1(\Omega)\otimes\mathbb{R}^2\otimes\mathbb{R}^2 \textit{ such that } \delta\Pi[\boldsymbol{u},\phi,\breve{\boldsymbol{u}}^x,\breve{\phi};\delta\boldsymbol{u},\delta\phi,\delta\breve{\boldsymbol{u}}^x,\delta\breve{\phi}]=0,
$$

$$
\forall(\delta\boldsymbol{u},\delta\phi,\delta\breve{\boldsymbol{u}}^x,\delta\breve{\phi})\in\mathcal{U}\otimes\mathcal{H}^1(\Omega)\otimes\mathbb{R}^2\otimes\mathbb{R}^2. \tag{41}
$$

4 | NUMERICAL APPROXIMATION AND CHOICE OF NUMERICAL PARAMETERS

The discretization of the weak form, Eq. (27) or (41), requires an approximation space for the displacement in $[\mathcal{H}^2(\Omega)]^d$ and with well-defined third derivatives on Dirichlet and periodicity boundaries. Here, following [8], we consider B-spline functions [40]. More precisely, we consider piecewise polynomial functions with C^{p-1} continuity, being $p\geq 3$ the degree of approximation. The uniform univariate B-splines basis is $\{B_i^p\}_{i=0}^{n_\xi-1}$ and it is defined in a parametric space $\xi\in[0,n_\xi+p]$ with the following recursive formula:

$$
B_i^0(\xi)=\begin{cases}1 & \xi_i\leq\xi<\xi_{i+1}\\ 0 & \text{otherwise}\end{cases};\qquad B_i^k(\xi)=\frac{\xi-\xi_i}{\xi_{i+k}-\xi_i}B_i^{k-1}(\xi)+\frac{\xi_{i+k+1}-\xi}{\xi_{i+k+1}-\xi_{i+1}}B_{i+1}^{k-1}(\xi);\qquad \begin{matrix}k=1,\dots,p\\ i=0,\dots,n_\xi+p-k-1,\end{matrix} \tag{42}
$$

where $\{\xi_i\}_{i=0}^{n_\xi-1}$ are the so-called knot points, here assumed to be not repeated and equispaced. An example of the unidimensional B-spline space is shown in Figure 4a. B-splines are defined in a multivariate by the tensor product of univariate ones, i.e.,

$$
B^p_{[i_\xi,i_\eta]}([\xi,\eta])=B^p_{i_\xi}(\xi)B^p_{i_\eta}(\eta);\quad i_\xi=0,\dots,n_\xi-1;\quad i_\eta=0,\dots,n_\eta-1. \tag{43}
$$

We consider a uniform Cartesian mesh embedding the domain Ω. Each cell of the mesh is classified in one of three disjoint groups: inner cells Ω^I, completely contained in the domain Ω, outer cells Ω^O, with null intersection with Ω, and cut cells Ω^C, that are cells intersected by the boundary $\partial\Omega$; as illustrated in the example in Figure 4b. Cut cells are divided into subdomains to perform the numerical integration using the algorithm described in Marco et al.[41,42]

Cut cells with very little intersection with Ω lead to ill-conditioned algebraic systems of equations[8] due to basis functions having a small contribution to the integral, and to basis functions being almost linearly dependent on those cells[43]. To alleviate this problem several strategies can be considered, such as the ghost-penalty method[44], the Extended B-spline method[45,46,47,48] or the artificial stiffness approach[49] among others. We use the extended B-spline method in this work. It consists on binding basis functions whose support is mostly outside of the geometry with adjacent basis functions. A detailed explanation about mesh creation and the numerical approach can be found in Codony et al.[8]

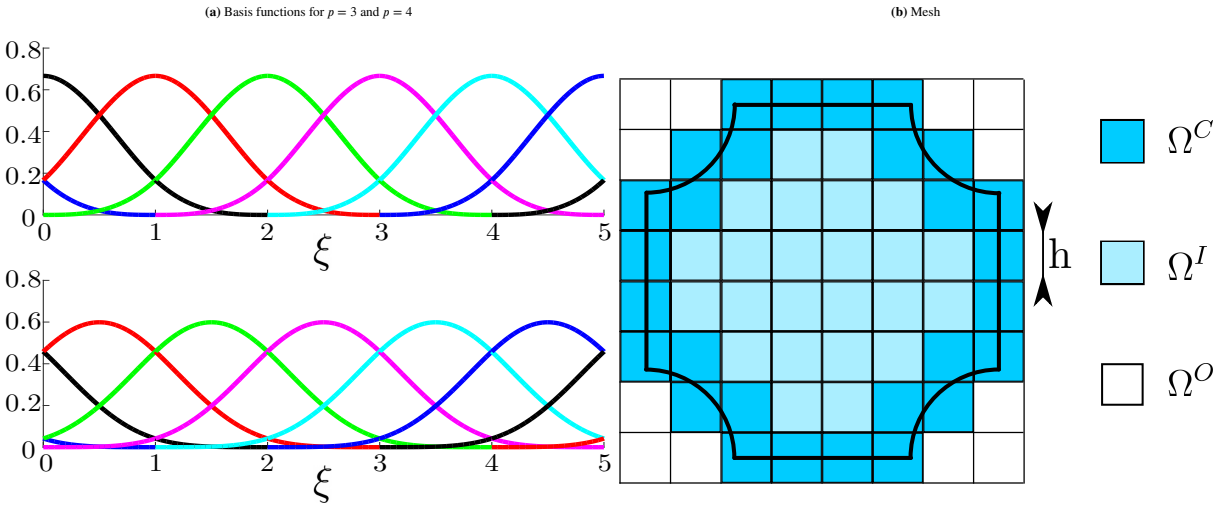

FIGURE 4 *a)* Unidimensional B-spline basis for degrees $p = 3$ and $p = 4$, *b)* Example of a mesh with inner cells in Ω^I, outer cells in Ω^O and cut cells in Ω^C.

The choice of the penalty parameters in Eqs. (7) and (17) follows[50,51,52,48,8]. We define the penalty parameters $\beta^u, \beta^v, \beta^{C_u}, \beta^\phi, \beta^{uI}, \beta^{vI}, \beta^{C_uI}, \beta^{\phi I} \in \mathbb{R}^+$ in terms of a *dimensionless* parameter $\zeta \in \mathbb{R}^+$ as

$$\beta^u = \frac{E}{h}\zeta, \qquad \beta^v = \frac{\ell^2 E}{h}\zeta, \qquad \beta^{C_u} = \frac{\ell^2 E}{h^2}\zeta, \qquad \beta^\phi = \frac{\epsilon}{h}\zeta, \tag{44}$$

$$\beta^{uI} = \frac{\max(E^{(1)}, E^{(2)})}{h}\zeta, \quad \beta^{vI} = \frac{\ell^2 \max(E^{(1)}, E^{(2)})}{h}\zeta, \quad \beta^{C_uI} = \frac{\ell^2 \max(E^{(1)}, E^{(2)}, ..., E^{(n)})}{h^2}\zeta, \quad \beta^{\phi I} = \frac{\max(\epsilon^{(1)}, \epsilon^{(2)})}{h}\zeta, \tag{45}$$

where h denotes the physical cell size of the mesh, and E, ϵ and ℓ denote the Young's modulus, the dielectric permittivity and the internal length scale arising from strain gradient elasticity, A. Thanks to the Extended B-splines stabilization, the penalty parameters do not depend on how the boundary intersects the mesh[47]. In any case, the value of ζ must be large enough for a well-defined system. Lower bounds can be derived by solving an eigenvalue problem[53,11,54]. A numerical study of the dependency of the condition number on the value of β can be found in Codony et al.[8]. A large value of ζ gives a poorly conditioned system that can deteriorate the performance of iterative solvers. Since we are using a direct solver for all numerical experiments, taking the optimal value of β is not critical.

Finally, we comment on the choice of the γ-parameter in Eqs. (13). Numerical oscillations around the interface may appear in some critical cases, when one element has a much smaller portion in one domain than in the other, as previously reported[12,36,55,56]. To improve the conditioning, we consider the following simplified version of parameters reported in Annavarapu et al. [36,56],

which yields accurate results:

$$\gamma^L = \frac{meas(S_{\Omega(L)})}{meas(S_{\Omega(L)}) + meas(S_{\Omega(R)})}, \qquad \gamma^R = \frac{meas(S_{\Omega(R)})}{meas(S_{\Omega(L)}) + meas(S_{\Omega(R)})}, \tag{46}$$

where $meas(S_{\Omega(i)})$ denotes the physical measure of the cut cell. The choice of the $\hat{\gamma}$-parameter in Eq. (14) is a generalization of the γ-parameters defined in Eq. (46) as

$$\hat{\gamma}^{P(k,i)} = \frac{meas(S_{\Omega(i)})}{\sum_{j=1}^{m(k)} meas(S_{\Omega(j)})} \tag{47}$$

For problems with large material constant ratios, it would be advisable to use a material-weighted definition of γ and β, analogous to that proposed by Dolbow et al. for elasticity [11,36,56]. Our selection of β and γ is not optimal, but it is sufficiently good to provide accurate results for the range of material parameters considered here. A generalization of the material-weighted definition of γ to electromechanical materials, as well as the study of the optimal value of γ, which would be particularly beneficial for iterative solvers, is beyond the scope of this paper.

5 | NUMERICAL EXPERIMENTS

Several numerical experiments are shown in this section. We first present error convergence analysis of the method on composite structures in 2D and 3D using dimensionless tests. A synthetic trigonometric solution is considered and optimal convergence in $\mathcal{L}^2$-norm is shown. In the third example we analyse a composite flexoelectric device. This device accumulates the flexoelectrically-generated electric bias by collective beam-bending avoiding internal cancelation of the effect thanks to the use of symmetry-breaking low-dielectricity inclusions [57,18]. The fourth example illustrates the efficiency and reliability of the proposed generalized periodicity approach. The solution in a unit cell with generalized periodicity in both directions is compared with the bulk response of a large structure formed by periodically replicating cells along the vertical direction. The last example compares the performance of several flexoelectric unit cells with different geometrical shapes under generalized periodicity conditions. For all the examples we use $\zeta = 10$ in Eqs. (44) and (45). That value gives accurate results for all the numerical experiments presented here using a direct solver.

5.1 | 2D Convergence Test

We consider the synthetic solution

$$\begin{aligned} u_x(x,y) &= \sin(2\pi x), \\ u_y(x,y) &= \sin(2\pi y), \\ \phi(x,y) &= \sin(2\pi x) + \sin(2\pi y), \end{aligned} \tag{48}$$

depicted in Fig. 5b on a three-material triangular domain of side 2, Fig. 5a. The corresponding material parameters are given in Table 1. We apply Dirichlet boundary conditions on the outer boundary $\partial\overline{\Omega}$ and at the corners C, consistent with the synthetic solution, and interface conditions on the material interfaces $\mathcal{I}$ and at the material interface corner $C^{\mathcal{I}}$. The precise interface conditions are given in Appendix B. The resulting numerical solution is then compared to the target synthetic solution.

Ω	E	ν	l	ϵ	$\boldsymbol{d}$	e_L	e_T	e_S	μ_L	μ_T	μ_S
1	152	0.33	1	141	$\mathbf{y}$	8.8	-4.4	4.4	1500	1100	1100
2	15	0.3	1	11	$\mathbf{y}$	3.8	-2.4	2.4	1100	100	100
3	19	0.25	1	85	$\mathbf{y}$	5.3	-3.2	2.6	100	1800	1800

TABLE 1 Material parameters for the 3 subdomains in Fig. 5a.

Figure 6 shows the convergence plots for the $\mathcal{L}^2$ norm, the $\mathcal{H}^1$ and $\mathcal{H}^2$ seminorms and for the error of the traction and electric charge density, for two different spline degrees, $p = 3$ and $p = 4$. The error on the interface is computed by integrating the square error on each interface for each one of the two values on the interface. The parameter $h_0 = 2$ is a normalization length

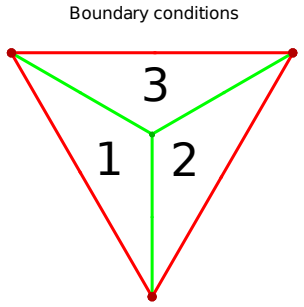

(a) Computational domain, material type and boundary.

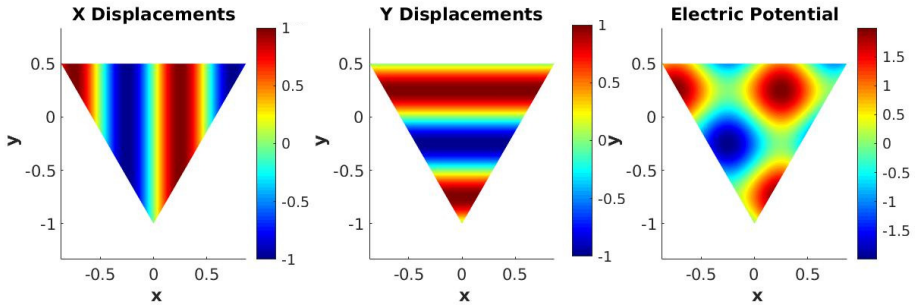

(b) Horizontal displacement, vertical displacement and electric potential.

FIGURE 5 a) Computational domain, where labels refer to material type of Table 1. The outer (Dirichlet) boundary $\partial\overline{\Omega}$ is shown in red, while material interfaces $\mathcal{I}$ are depicted in green. Boundary corners C and the interior corner $C^{\mathcal{I}}$ are marked with a darker color. b) Target synthetic solution, Eq. (48).

and $\log_2(h_0/h)$ is the mesh refinement level. In each simulation we are dividing h by 2. Optimal convergence is obtained in all cases. For simplicity we will use B-spline of degree $p = 3$ in the following examples.

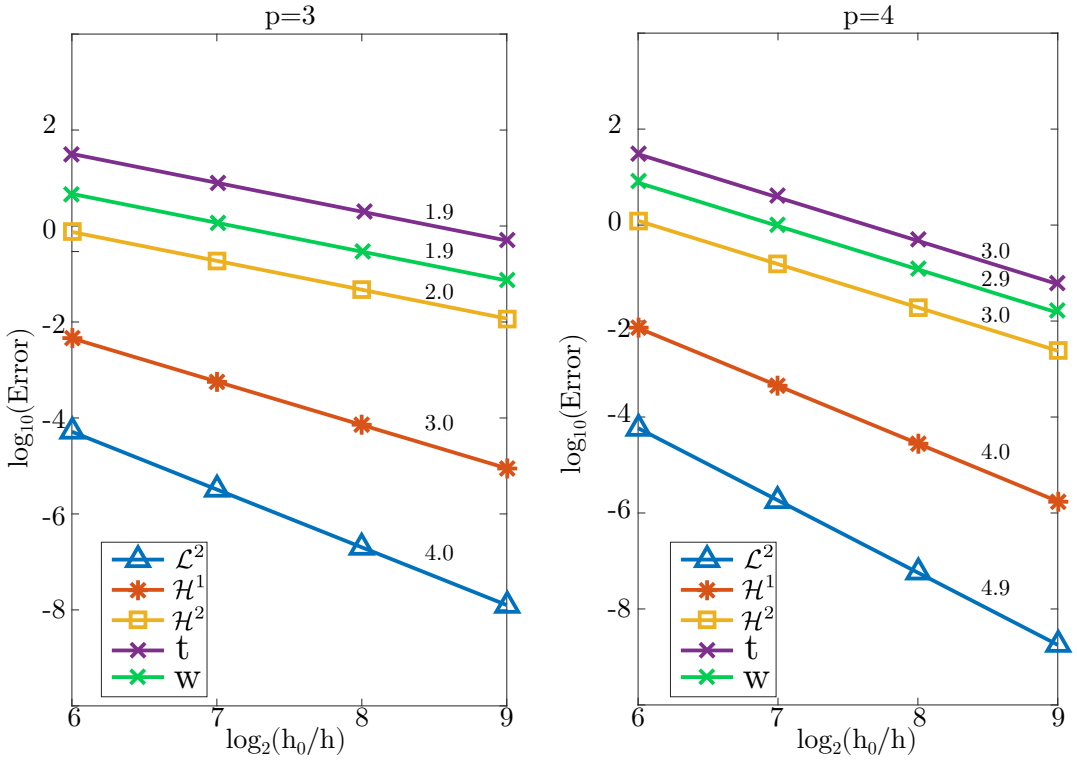

FIGURE 6 Convergence plots for the $\mathcal{L}^2$ norm, the $\mathcal{H}^1$ and $\mathcal{H}^2$ seminorms and for the error of the traction and electric charge density, for two different spline degrees, $p = 3$ (left) and $p = 4$ (right)

5.2 | 3D Convergence Test

We now test convergence in a three-dimensional domain formed by four cubes of size 2x2x2 of two different set of values of material parameters, Table 1, jointly forming the parallelepiped shown in Fig. 7. We impose Dirichlet boundary conditions on

the outer boundaries $\partial\overline{\Omega}$ and edges C and interface conditions on the interfaces $\mathcal{I}$ and interface edges $C^{\mathcal{I}}$ consistent with the synthetic solution

$$
\begin{aligned}
u_x(x,y,z) &= \sin(0.1x),\\
u_y(x,y,z) &= \cos(0.1y),\\
u_z(x,y,z) &= 0.5\cos(0.1y) + \sin(0.1z),\\
\phi(x,y,z) &= 3\sin(0.1x) - 4\cos(0.1y) + 7\sin(0.1z).
\end{aligned} \tag{49}
$$

The precise interface conditions are given in Appendix B. The $\mathcal{L}^2$ norm, the $\mathcal{H}^1$ and $\mathcal{H}^2$ seminorms and for the error of the traction and electric charge density of the numerical solution with respect to the synthetic solutions are plotted in Fig. 7, for B-spline discretization of degree $p = 3$ and normalization length $h_0 = 4$. In each simulation we are dividing the mesh size h by 2. Optimal convergence is obtained in all cases.

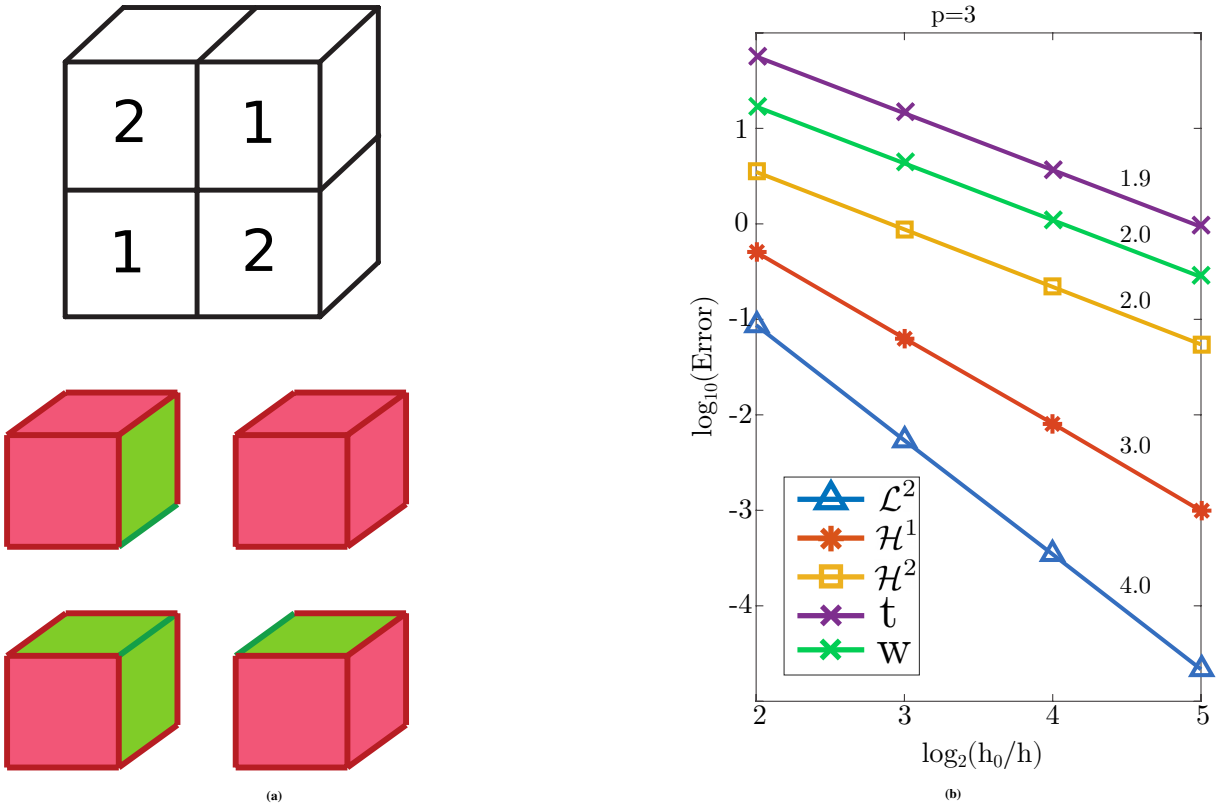

FIGURE 7 a) Computational domain (top) and boundary conditions (bottom). Labels indicate material type. Dirichlet boundaries are depicted in red and interfaces are depicted in green. The edges are depicted with a darker color. b) Convergence plot for the $\mathcal{L}^2$ norm, the $\mathcal{H}^1$ and $\mathcal{H}^2$ seminorms and for the error of the traction and electric charge density, with degree $p = 3$ and normalization length $h_0 = 4$. The number for each plot is the slope of the last segment.

Ω	E	ν	l	ϵ	$\boldsymbol{d}$	e_L	e_T	e_S	μ_L	μ_T	μ_S
1	152	0.33	1	141	**z**	8.8	-4.4	4.4	1500	1100	1100
2	15	0.3	1	11	**z**	3.8	-2.4	2.4	1100	100	100

TABLE 2 Material parameters for the 4 subdomains in Figure 7.

5.3 | Comb-like flexoelectric harvester

We consider next an electromechanical device consisting in two comb-like structures of non-piezoelectric dielectric joint together by a low-dielectricity material by the tip of the beams, Fig. 8a. The application of a shear motion at the left and right sides of the structure, induces beam bending and triggers locally the flexoelectric effect. This local flexoelectrically generated electric potential is accumulated through the structure, as shown in Fig. 8b. By breaking the overall centrosymmetry of the system, the low-dielectricity material inclusions preclude internal cancelation of the local flexoelectrically generated electric potential, thereby endowing the device with an effective piezoelectric behavior, even when the base material is a non-piezoelectric dielectric[31,18,19].

A 10-beam device is considered, for illustration purposes. The beams are 100 nm long by 10 nm wide, the insulator is a square of side 10 nm. Material properties are given in Table 3. Displacements, $\boldsymbol{u}_L = (0, 5)$ nm and $\boldsymbol{u}_R = (0, -5)$ nm are prescribed on the left and right sides of the structure, and the top-right half side of the structure is electrically grounded, Fig. 8a. Homogeneous Neumann boundary conditions are assumed otherwise. The effective piezoelectric response of the structure manifests in a net potential difference between the ground electrode and the top-left half side of the structure.

Ω	E[GPa]	ν	l[nm]	ϵ[nJ V^{-2} m^{-1}]	$\boldsymbol{d}_{\text{piezo}}$	e_L[J V^{-1} m^{-2}]	e_T	e_S	μ_L[μJ V^{-1} m^{-1}]	μ_T	μ_S
1	152	0.33	1	141	$\mathbf{y}$	0	0	0	150	110	110
2	152	0.33	1	141×10^{-7}	$\mathbf{y}$	0	0	0	0	0	0

TABLE 3 Material properties of the material tensors described in Section 5.3

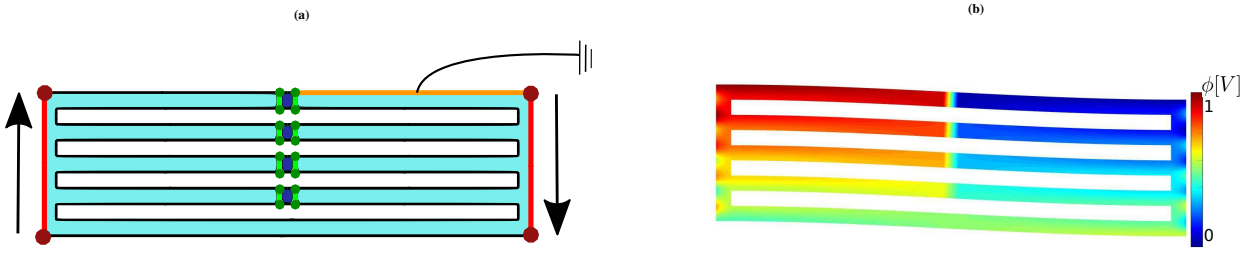

FIGURE 8 (a) Geometry of the comb with flexoelectric material in Ω_1 (in light blue) and insulator in Ω_2 (in dark blue). The interface, $\mathcal{I}$, and its corners, $\mathcal{C}$, are also shown in green. Dirichlet boundary is depicted in red and electrical ground side is shown is orange. (b) Deformed shape of the material and electric potential distribution.

5.4 | Generalized periodicity analysis: sensor under vertical compression.

We validate the generalized periodicity conditions by comparing the response of a large periodic arrangement of triangular voids on a dielectric matrix to that of the periodic unit cell, Fig. 9. Such structure has been proposed as a means to generate local flexoelectric response in a non-piezoelectric material in such a way that a net electric potential is generated under macroscopic homogeneous deformation[31,18]. For a very large structure under a prescribed strain, we expect the solution in the central part of the structure to be unaffected by boundary effects and thus exhibiting generalized periodicity. In Fig. 9, we compare the solution obtained on the generalized periodic unit cell with the central unit cell of a vertical stack of N unit cells. In the first simulation, we consider a unit cell with generalized periodic conditions in both directions. A displacement jump along the vertical direction y

$$\hat{\boldsymbol{u}}^y = (0, -0.1) \text{ nm}. \tag{50}$$

is prescribed and all other jumps in Eq. (28), $\check{\boldsymbol{u}}^x$, $\check{\phi}^x$ and $\check{\phi}^y$, are let free, see discussion under Eq. (29). The unit cell is a square of side 4 μm with a triangular void of side $\frac{3\sqrt{3}}{2}$μm. The material properties correspond to the first material in Table 3. Figure

9a shows the unit cell and the resulting electric potential distribution. In the second simulation, we consider a stack of N=19 such unit cells subject to prescribed displacements on the top and bottom faces matching, in the limit, the previous generalized periodicity conditions, i.e.

$$\boldsymbol{u}|_{y=y_{max}} = N\hat{\boldsymbol{u}}^y \qquad \boldsymbol{u}|_{y=0} = \boldsymbol{0}, \tag{51}$$

and unconstrained generalized periodicity conditions for $\boldsymbol{u}$ and ϕ in the horizontal direction. As the electric potential is determined up to a constant, we set it to zero at the center of the structure. Figure 9b shows the vertical structure and the electric potential distribution, with a zoom around the central cell. For comparison purposes, the scale of the electric potential for the second simulation is adjusted to show perfect agreement with the generalized periodic unit cell result, Fig. 9a. That error is smaller than 0.1% in all points inside the unit cell. For stacks of a large number of unit cells, we expect the average electric

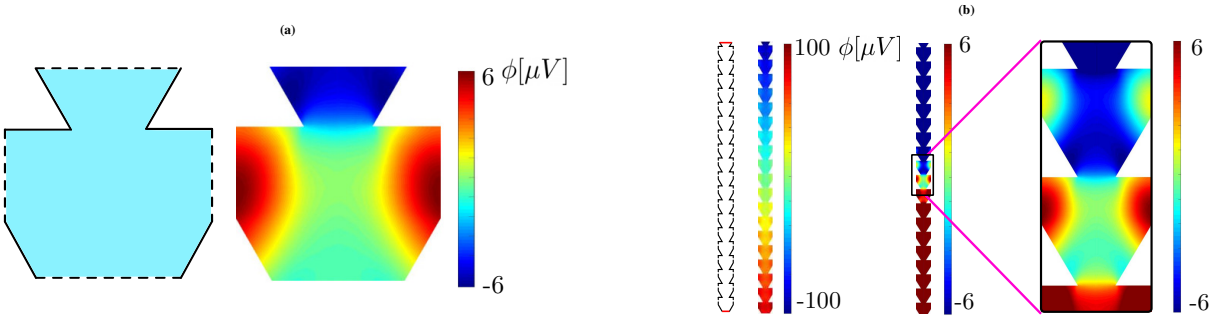

FIGURE 9 (a) Unit cell and electric potential distribution with generalized periodic conditions in both directions. (b) Distribution of the electric potential in a structure formed by 19 unit cells prescribed displacements at the top and bottom. Results on the central generalized periodic unit cell are shown with the same scale as a) for direct comparison purposes.

potential difference on a unit cell to tend to the generalized periodicity electric potential jump $\check{\phi}^y$, i.e.

$$\lim_{N\to\infty} \frac{\overline{\Delta\phi}}{N} = \check{\phi}^y, \tag{52}$$

where $\overline{\Delta\phi}$ is the electric potential difference between top and bottom boundaries of the structure in Fig. 9b. For quantitative validation purposes, we plot in Fig. 10 the value of $\overline{\Delta\phi}/N$ for stacks of increasing number of unit cells, from $N = 1$ to $N = 20$ and compare it against the generalized periodicity electric potential jump $\check{\phi}^y$ obtained in the generalized periodic unit cell simulation, Fig. 9b. From this plot, the limit in Eq. (52) is apparent. The electromechanical response of a unit cell under generalized periodicity conditions is thus shown to be representative of the bulk response of a periodic material built from that unit cell under the corresponding macroscopic conditions on its boundaries. Although we only show the validation for a sensor mode considering generalized periodicity in y-direction, actuator mode and different generalized periodicity have been considered and all them have the same agreement as the one presented here.

5.5 | Unit cell of flexoelectric metamaterial in sensor mode.

We now analyze the performance of three 2D periodic structures with periodically-replicated holes. As shown in Figure 11a, the unit cells are a square of side 4 µm with holes of different shapes: a square of side 1 µm, a triangle of side $\frac{3\sqrt{3}}{2}$µm and and circle of radius 1 µm. The material is a non-piezoelectric dielectric with properties corresponding to the first material in Table 3. The generalized periodicity conditions used are

$$\hat{\boldsymbol{u}}^y = (0, -0.1)\ \ \mu\text{m}, \tag{53}$$

while all other generalized periodicity jumps, $\check{\boldsymbol{u}}^x$, $\check{\phi}^x$ and $\check{\phi}^y$, are let free. This corresponds to applying a uniform compressive strain in the vertical direction at the macroscopic level, while allowing a free transversal expansion or compression of the material. As the solution is determined up to a constant, the displacement and the electric potential of the most left down corner is set to 0. If the resulting $\check{\phi}^y$ is not null, the potential difference accumulates with the repetition of unit cells and the flexoelectric metamaterial behaves effectively as a piezoelectric at the macroscale.

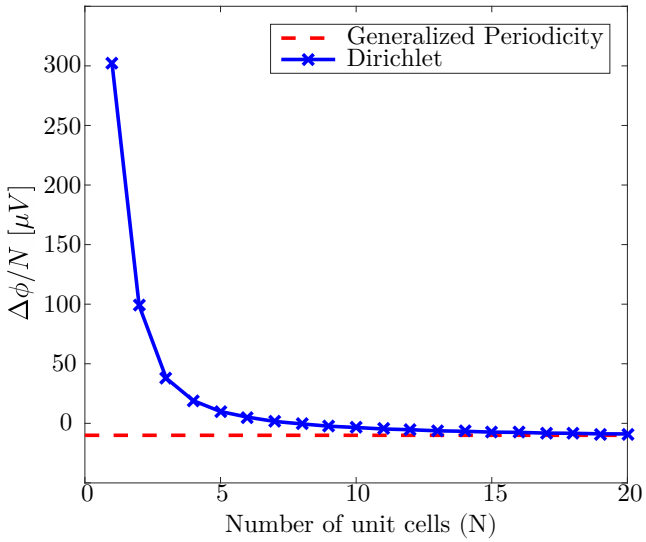

FIGURE 10 Plot of the difference of electric potential, $\Delta\phi$, per unit cell, versus the number of unit cells N (in blue) and potential difference, $\check{\phi}^y$, for one unit cell considering generalized periodicity in both directions (in red).

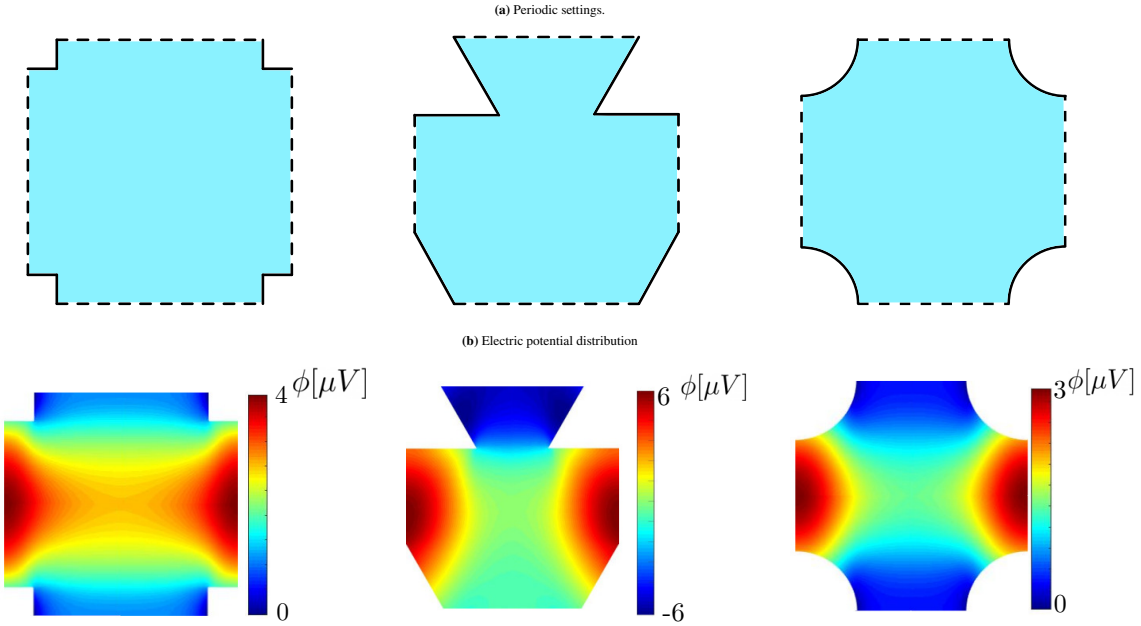

FIGURE 11 (a) Periodic unit cell of a metamaterial with square, triangular and circular holes respectively (b) Distribution of the electric potential in the unit cells.

From Figure 11b, we see that centro-symmetric structures, namely those with square and circular holes, do not lead to a net electric potential accumulation. On the other hand, the non-centrosymmetric structure with a triangular hole leads to a net electric potential difference. Therefore, the triangular hole can be used to create a flexoelectric metamaterial, in agreement with[58,18].

6 | CONCLUDING REMARKS

In this paper we propose a formulation for simulating general flexoelectric domains composed by multiple materials in unfitted meshes. Boundary conditions and interface conditions are imposed in weak form through a variational formulation following

Nitsche's method. The high-order continuity required by the resulting weak form is fulfilled by using an unfitted B-spline approximation. Optimal convergence is demonstrated with numerical tests in 2D and 3D.

The proposed method is also particularized to the modelling of flexoelectricity problems in generalized periodic structures. Periodicity boundaries are treated as mathematical interfaces and the variational formulation is used to weakly impose generalized periodicity conditions. The formulation is tested on a geometrically periodic structure under applied macroscopic strain. The electromechanical response of the generalized periodic unit cell under generalized periodicity conditions is shown to be representative of the bulk response of large geometrically periodic structures. Three examples of periodic structures are shown to illustrate the applicability and efficiency of the proposed formulation to analyze and design flexoelectric metamaterials.

Although we focus here mainly on flexoelectricity with strain gradient elasticity, the formulation is readily extensible to other high-order problems. The reduction to the computation of one unit cell of a periodic structure makes this method really useful for computational homogenization.

ACKNOWLEDGMENTS

This work was supported by the Generalitat de Catalunya ("ICREA Academia" award for excellence in research to I.A., and Grant No. 2017-SGR-1278), the European Research Council (StG-679451 to I.A.) and Departament de Recerca i Universitats de la Generalitat de Catalunya. CIMNE is a recipient of a "Severo Ochoa Programme for Centres of Excellence in R&D" grant (CEX2018-000797-S) by the Spanish Ministry of Economy and Competitiveness. Helpful discussion with O. Marco is gratefully acknowledged.

How to cite this article: Barceló-Mercader J., D. Codony, S. Fernández-Méndez, and I. Arias (2021), Weak enforcement of interface continuity and generalized periodicity in high-order electromechanical problems,

APPENDIX

A MATERIAL TENSORS

In the following appendix, the material tensors are defined, as in Codony et al.[8]. They are described component-wise (non-zero components) and d is the number of dimensions of the physical space.

We use an isotropic elasticity tensor defined in terms of the Young modulus E and Poisson ratio ν as

$$\begin{aligned} \mathbb{C}_{iiii} &= C_L, && i = 1, \dots, d; \\ \mathbb{C}_{iijj} &= C_T, && i, j = 1, \dots, d \ : \ i \neq j; \\ \mathbb{C}_{ijij} = \mathbb{C}_{ijji} &= C_S, && i, j = 1, \dots, d \ : \ i \neq j, \end{aligned} \tag{A1}$$

where the parameters C_L, C_S and C_T are

$$C_L := \frac{E\,(1-\nu)}{(1+\nu)(1-2\nu)}, \qquad C_T := \frac{E\nu}{(1+\nu)(1-2\nu)}, \qquad C_S := \frac{E}{2(1+\nu)} \tag{A2}$$

We use a sixth-order tensor to describe strain gradient elasticity. We consider an isotropic version of the general model in Mindlin et al.[59] that is described in Atlan et al.[60]. The strain gradient tensor depends on the Young modulus E, the Poisson ratio ν and the internal length scale ℓ as

$$\begin{aligned} h_{iikiik} &= \ell^2 C_L, && i, k = 1, \dots, d; \\ h_{iikjjk} &= \ell^2 C_T, && i, j, k = 1, \dots, d \ : \ i \neq j; \\ h_{ijkijk} = h_{ijkjik} &= \ell^2 C_S, && i, j, k = 1, \dots, d \ : \ i \neq j \end{aligned} \tag{A3}$$

where the parameters C_L, C_S and C_T are defined in Eq. (A2).

We use an second-order tensor to describe isotropic dielectricity ϵ, which depends on a parameter as

$$\epsilon_{ii} = \epsilon, \qquad i = 1, \dots, d. \tag{A4}$$

Piezoelectricity is represented by the third-order tensor $\boldsymbol{e}$, where tetragonal symmetry is considered, which has a principal direction. It involves longitudinal, transversal and shear couplings represented by the parameters e_L, e_T and e_S, respectively. For a material with principal direction $\boldsymbol{x}_1$, the piezoelectric tensor $\boldsymbol{e}^{<\boldsymbol{x}_1>}$ is

$$\begin{aligned} e^{<\boldsymbol{x}_1>}{}_{111} &= e_L; \\ e^{<\boldsymbol{x}_1>}{}_{1jj} &= e_T, && j = 2, \dots, d; \\ e^{<\boldsymbol{x}_1>}{}_{j1j} = e^{<\boldsymbol{x}_1>}{}_{jj1} &= e_S, && j = 2, \dots, d. \end{aligned} \tag{A5}$$

The piezoelectric tensor $\boldsymbol{e}$ oriented in an arbitrary direction $\boldsymbol{d}$ is obtained by rotating $\boldsymbol{e}^{<\boldsymbol{x}_1>}$. Flexoelectricity is represented by the fourth-order tensor $\boldsymbol{\mu}$ where cubic symmetry is considered. It leads to a tensor involving longitudinal, transversal and shear couplings represented by the parameters μ_L, μ_T and μ_S, respectively. The components of the flexoelectric tensor $\boldsymbol{\mu}^{<\boldsymbol{x}>}$ of a material oriented in the Cartesian axes are the following:

$$\begin{aligned} \mu^{<\boldsymbol{x}>}{}_{iiii} &= \mu_L, && i = 1, \dots, d; \\ \mu^{<\boldsymbol{x}>}{}_{ijji} &= \mu_T, && i, j = 1, \dots, d \ : \ i \neq j; \\ \mu^{<\boldsymbol{x}>}{}_{iijj} = \mu^{<\boldsymbol{x}>}{}_{ijij} &= \mu_S, && i, j = 1, \dots, d \ : \ i \neq j. \end{aligned} \tag{A6}$$

The flexoelectric tensor $\boldsymbol{\mu}$ oriented in an arbitrary orthonormal basis is obtained by rotating $\boldsymbol{\mu}^{<\boldsymbol{x}>}$.

B SPECIFIC INTERFACE CONDITION FOR SYNTHETIC SOLUTION

In the following appendix the specific interface conditions for sections 5.1 and 5.2 are detailed. The synthetic solution for section 5.1 is

$$u_x = \sin(2\pi x), \quad u_y = \sin(2\pi y), \quad \phi = \sin(2\pi x) + \sin(2\pi y). \tag{B7}$$

The body force and free charges are

$$\begin{aligned} q &= \left[4\pi^2\epsilon\right]\sin(2\pi x) - \left[4\pi^2(e_T - \epsilon)\right]\sin(2\pi y) - \left[8\pi^3\mu_L\right]\cos(2\pi x) - \left[8\pi^3\mu_L\right]\cos(2\pi y), \\ b_x &= \left[C_L(16\ell\pi^4 + 4\pi^2)\right]\sin(2\pi x) - \left[8\pi^3\mu_L\right]\cos(2\pi x), \\ b_y &= \left[4\pi^2 e_S\right]\sin(2\pi x) + \left[16\pi^4\ell^2 C_L + C_L + e_L\right]\sin(2\pi y)) - \left[8\pi^3\mu_L\right]\cos(2\pi y), \end{aligned} \tag{B8}$$

and the traction, double traction, electric charge density and edge forces are

$$\begin{aligned} t_x =& \left[-4\pi n_1(\mu_L n_1^2 + \mu_S n_2^2 - 2\mu_L)\right]\sin(2\pi x) + \left[4\pi^2 n_1^3(\mu_S + \mu_T)\right]\sin(2\pi y) \\ &+ \left[-8\pi^3 C_L\ell^2 n_1^3 + 16\pi^3 C_L\ell^2 n_1 + 4\pi C_L n_1 + 2\pi n_2 e_S\right]\cos(2\pi x) \\ &+ \left[8\pi^3 n_1^3\ell^2 C_T + 2\pi n_1 C_T + 2\pi n_1 e_T\right]\cos(2\pi y), \\ t_y =& \left[4\pi^2 n_2^3(\mu_S + \mu_T)\right]\sin(2\pi x) - \left[4\pi n_2(\mu_L n_2^2 + \mu_S n_1^2 - 2\mu_L)\right]\sin(2\pi y) \\ &+ \left[8\pi^3 n_2^3\ell^2 C_T + 2\pi n_2 C_T + 2\pi n_2 e_T\right]\cos(2\pi x) \\ &+ \left[-8\pi^3 C_L\ell^2 n_2^3 + 16\pi^3 C_L\ell^2 n_2 + 4\pi C_L n_2 + 2\pi n_1 e_S\right]\cos(2\pi y), \\ r_x =& \left[-4\pi^2\ell^2 n_1^2 C_L\right]\sin(2\pi x) - \left[4\pi^2\ell^2 C_T n_1 n_2\right]\sin(2\pi y) + \left[2\pi\mu_S n_2^2 + 2\pi\mu_L n_1^2\right]\cos(2\pi x) + \left[2\pi(\mu_S + \mu_T)n_1 n_2\right]\cos(2\pi y), \\ r_y =& \left[-4\pi^2\ell^2 C_T n_1 n_2\right]\sin(2\pi x) - \left[4\pi^2\ell^2 n_2^2 C_L\right]\sin(2\pi y) + \left[2\pi(\mu_S + \mu_T)n_1 n_2\right]\cos(2\pi x) + \left[2\pi\mu_S n_1^2 + 2\pi\mu_L n_2^2\right]\cos(2\pi y), \\ w =& \left[4\pi^2\mu_L n_1\right]\sin(2\pi x) - \left[2\pi n_2\right]\sin(2\pi y) - \left[2\pi(e_L n_2 - \epsilon n_1)\right]\cos(2\pi x) - \left[2\pi n_2(e_T - \epsilon)\right]\cos(2\pi y), \\ j_x =& -\left[4\pi^2\ell^2 C_L(m_1^L n_1^L + m_1^R n_1^R)\right]\sin(2\pi x) - \left[4\pi^2\ell^2 C_T(m_1^L n_2^L + m_1^R n_2^R)\right]\sin(2\pi y) \\ &+ \left[2\pi(m_1^L n_1^L\mu_L + m_1^R n_1^R\mu_L + \mu_S(m_2^L n_2^L + m_2^R n_2^R))\right]\cos(2\pi x) \\ &+ \left[2\pi(m_1^L n_1^L\mu_T + m_1^R n_2^R\mu_T + \mu_S(m_2^L n_1^L + m_2^R n_1^R))\right]\cos(2\pi y), \\ j_y =& \left[-4\pi^2\ell^2 C_T(m_2^L n_1^L + m_2^R n_1^R)\right]\sin(2\pi x) - \left[4\pi^2\ell^2 C_L(m_2^L n_2^L + m_2^R n_2^R)\right]\sin(2\pi y) \\ &+ \left[2\pi(m_2^L n_2^L\mu_T + m_2^R n_1^R\mu_T + \mu_S(m_1^L n_2^L + m_1^R n_2^R))\right]\cos(2\pi x) \\ &+ \left[2\pi(m_2^L n_2^L\mu_L + m_2^R n_2^R\mu_L + \mu_S(m_1^L n_1^L + m_1^R n_1^R))\right]\cos(2\pi y), \end{aligned} \tag{B9}$$

where $\mathbf{n} = (n_1, n_2)^T$

The synthetic solution for section 5.2 is

$$u_x = \sin(0.1x), \quad u_y = \cos(0.1y), \quad u_z = 0.5\cos(0.1y) + \sin(0.1z), \quad \phi = 3\sin(0.1x) - 4\sin(0.1y) + 7\sin(0.1z). \tag{B10}$$

The body force and free charges are

$$\begin{aligned}
q =& \left[0.03\epsilon\right]\cos(0.1x) + \left[0.001\mu_L\right]\sin(0.1y) + \left[0.07\epsilon - 0.01e_L\right]\sin(0.1z)\\
&- \left[0.001\mu_L\right]\cos(0.1x) + \left[-0.04\epsilon - 0.005e_S\right]\cos(0.1y) - \left[0.001\mu_L\right]\cos(0.1z),\\
b_x =& \left[(0.01 + 0.0001\ell^2)C_L\right]\sin(0.1x) - \left[0.003\mu_L\right]\cos(0.1x),\\
b_y =& \left[(0.01 + 0.0001\ell^2)C_L\right]\cos(0.1y) - \left[0.004\mu_L\right]\sin(0.1y),\\
b_z =& \left[0.03e_S\right]\sin(0.1x) + \left[0.07e_L + 0.01C_L + 0.0001\ell^2 C_L\right]\sin(0.1z)\\
&+ \left[(0.005 + 0.00005\ell^2)C_S - 0.04e_S\right]\cos(0.1y) - \left[0.007\mu_L\right]\cos(0.1z).
\end{aligned} \tag{B11}$$

The traction, double traction, electric charge density and edge forces are

$$\begin{aligned}
t_x =& \left[-0.05\mu_L n_1^3 + ((-0.03n_2^2 - 0.03n_3^2)\mu_S + 0.06\mu_L)n_1)\right]\sin(0.1x)\\
&+ \left[(-0.1 + (0.001n_2^2 - 0.001)\ell^2)C_T n_1\right]\sin(0.1y)\\
&+ \left[((0.07 - 0.07n_3^2)\mu_S - 0.07n_3^2\mu_T + 0.07\mu_T)n_1\right]\sin(0.1z)\\
&+ \left[-0.001C_L\ell^2 n_1^3 + (0.002\ell^2 C_L + 0.1C_L)n_1 + 0.3e_S n_3\right]\cos(0.1x)\\
&+ \left[(-0.04\mu_S + 0.04n_2^2\mu_T + 0.04n_2^2\mu_S - 0.04\mu_T)n_1\right]\cos(0.1y)\\
&+ \left[((0.1 + (-0.001n_3^2 + 0.001)\ell^2)C_T + 0.7e_T)n_1\right]\cos(0.1z),\\
t_y =& \left[(0.03\mu_T + 0.03\mu_S - 0.03n_1^2\mu_T - 0.03\mu_S n_1^2)n_2\right]\sin(0.1x)\\
&+ \left[0.001C_L\ell^2 n_2^3 + 0.0005\ell^2 C_S n_2^2 n_3 + (-0.002\ell^2 C_L - 0.1C_L)n_2 + (0.4e_S - 0.05C_S - 0.0005\ell^2 C_S)n_3\right]\sin(0.1y)\\
&+ \left[((-0.07\mu_T - 0.07\mu_S)n_3^2 + 0.07\mu_T + 0.07\mu_S)n_2\right]\sin(0.1z)\\
&+ \left[((0.001 - 0.001n_1^2)C_T\ell^2 + 0.1C_T)n_2\right]\cos(0.1x)\\
&+ \left[0.04\mu_L n_2^3 + (-0.08\mu_L + 0.04\mu_S n_1^2 + 0.04\mu_S n_3^2)n_2\right]\cos(0.1y)\\
&+ \left[(0.1C_T - 0.001C_T n_3^2\ell^2 + 0.001C_T\ell^2 + 0.7e_T)n_2\right]\cos(0.1z),\\
t_z =& \left[((0.03 - 0.03n_1^2)\mu_S + 0.03\mu_T - 0.03n_1^2\mu_T)n_3\right]\sin(0.1x)\\
&+ \left[(0.001n_2^2\ell^2 C_T - 0.001C_T\ell^2 - 0.1C_T)n_3 + 0.0005C_S\ell^2 n_2^3 + (-0.001\ell^2 C_S - 0.05C_S + 0.4e_S)n_2\right]\sin(0.1y)\\
&+ \left[-0.07\mu_L n_3^3 + (-0.07n_2^2\mu_S - 0.07\mu_S n_1^2 + 0.14\mu_L)n_3\right]\sin(0.1z)\\
&+ \left[((0.001 - 0.001n_1^2)C_T\ell^2 + 0.1C_T)n_3 + 0.3e_S n_1\right]\cos(0.1x)\\
&+ \left[((0.04\mu_T + 0.04\mu_S)n_2^2 - 0.04\mu_S - 0.04\mu_T)n_3\right]\cos(0.1y)\\
&+ \left[-0.001C_L\ell^2 n_3^3 + (0.002\ell^2 C_L + 0.1C_L + 0.7e_L)n_3\right]\cos(0.1z),\\
r_x =& \left[-0.01n_1^2\ell^2 C_L\right]\sin(0.1x) + \left[(0.4\mu_T n_2 + 0.4n_2\mu_S)n_1\right]\sin(0.1y) - \left[0.01n_1 n_3\ell^2 C_T\right]\sin(0.1z)\\
&+ \left[0.3n_1^2\mu_L + (0.3n_2^2 + 0.3n_3^2)\mu_S\right]\cos(0.1x) - \left[0.01n_1 n_2\ell^2 C_T\right]\cos(0.1y) + \left[(0.7n_3\mu_T - 0.7\mu_S n_3)n_1\right]\cos(0.1z),\\
r_y =& \left[-0.01n_1 n_2\ell^2 C_T\right]\sin(0.1x) + \left[0.4\mu_S n_1^2 + 0.4\mu_L n_2^2 + 0.4\mu_S n_3^2\right]\sin(0.1y) - \left[0.01n_2 n_3\ell^2 C_T\right]\sin(0.1z)\\
&+ \left[(0.3\mu_S n_1 + 0.3n_1\mu_T)n_2\right]\cos(0.1x) + \left[-0.01n_2^2\ell^2 C_L - 0.005n_2 n_3\ell^2 C_S\right]\cos(0.1y) + \left[(0.7\mu_T + 0.7\mu_S)n_2 n_3\right]\cos(0.1z),\\
r_z =& \left[-0.01n_1 n_3\ell^2 C_T\right]\sin(0.1x) + \left[(0.4\mu_T + 0.4\mu_S)n_2 n_3\right]\sin(0.1y) - \left[0.01n_3^2\ell^2 C_L\right]\sin(0.1z)\\
&+ \left[(0.3\mu_S n_1 + 0.3\mu_T n_1)n_3\right]\cos(0.1x) + \left[-0.005n_2^2\ell^2 C_S - 0.01n_2 n_3\ell^2 C_T\right]\cos(0,1y)\\
&+ \left[0.7\mu_S n_1^2 + 0.7n_2^2\mu_S + 0.7n_3^2\mu_L\right]\cos(0.1z),\\
w =& \left[0.01n_1\mu_L\right]\sin(0.1x) + \left[0.4n_2\epsilon + 0.05e_S n_2 + 0.1e_T n_3\right]\sin(0.1y) + \left[0.01n_3\mu_L\right]\sin(0.1z)\\
&+ \left[0.3n_1\epsilon - 0.1e_T n_3\right]\cos(0.1x) + \left[0.01\mu_L n_2 + 0.005\mu_S n_3\right]\cos(0.1y) + \left[(0.7\epsilon - 0.1e_L)n_3\right]\cos(0.1z),
\end{aligned} \tag{B12}$$

$$
\begin{aligned}
j_x =& \left[-0.01C_L\ell^2 m_1^L n_1^L - 0.01C_L\ell^2 m_1^R n_1^R \right] \sin(0.1x) \\
&+ \left[(0.4m_2^L n_1^L + 0.4m_2^R n_1^R)\mu_S + 0.4m_1^L n_2^L \mu_T + 0.4m_1^R n_2^R \mu_T \right] \sin(0.1y) \\
&+ \left[-0.01C_T\ell^2 m_1^L n_3^L - 0.01C_T\ell^2 m_1^R n_3^R \right] \sin(0.1z) \\
&+ \left[(0.3m_2^L n_2^L + 0.3m_2^R n_2^R + 0.3m_3^L n_3^L + 0.3m_3^R n_3^R)\mu_S + 0.3m_1^L n_1^L \mu_L + 0.3m_1^R n_1^R \mu_L \right] \cos(0.1x) \\
&+ \left[-0.01C_T\ell^2 m_1^L n_2^L - 0.01C_T\ell^2 m_1^R n_2^R \right] \cos(0.1y) \\
&+ \left[(0.7m_3^L n_1^L + 0.7m_3^R n_1^R)\mu_S + 0.7m_1^L n_3^L \mu_T + 0.7m_1^R n_3^R \mu_T \right] \cos(0.1z), \\
j_y =& \left[(-0.01C_T m_2^L n_1^L - 0.01C_T m_2^R n_1^R)\ell^2 \right] \sin(0.1x) \\
&+ \left[(0.4m_1^L n_1^L + 0.4m_1^R n_1^R + 0.4m_3^L n_3^L + 0.4m_3^R n_3^R)\mu_S + 0.4m_2^L n_2^L \mu_L + 0.4m_2^R n_2^R \mu_L \right] \sin(0.1y) \\
&+ \left[(-0.01C_T m_2^L n_3^L - 0.01C_T m_2^R n_3^R)\ell^2 \right] \sin(0.1z) \\
&+ \left[(0.3m_1^L n_2^L + 0.3m_1^R n_2^R)\mu_S + 0.3m_2^L n_1^L \mu_T + 0.3m_2^R n_1^R \mu_T \right] \cos(0.1x) \\
&+ \left[(-0.01C_L m_2^L n_2^L - 0.01C_L m_2^R n_2^R - 0.005C_S m_3^L n_2^L - 0.005C_S m_3^R n_2^R)\ell^2 \right] \cos(0.1y) \\
&+ \left[(0.7m_3^L n_2^L + 0.7m_3^R n_2^R)\mu_S + 0.7m_2^L n_3^L \mu_T + 0.7m_2^R n_3^R \mu_T \right] \cos(0.1z), \\
j_z =& \left[(-0.01C_T m_3^L n_1^L - 0.01C_T m_3^R n_1^R)\ell^2 \right] \sin(0.1x) \\
&+ \left[(0.4m_2^L n_3^L + 0.4m_2^R n_3^R)\mu_S + 0.4m_3^L n_2^L \mu_T + 0.4m_3^R n_2^R \mu_T \right] \sin(0.1y) \\
&+ \left[(-0.01C_L m_3^L n_3^L - 0.01C_L m_3^R n_3^R)\ell^2 \right] \sin(0.1z) \\
&+ \left[(0.3m_1^L n_3^L + 0.3m_1^R n_3^R)\mu_S + 0.3m_3^L n_1^L \mu_T + 0.3m_3^R n_1^R \mu_T \right] \cos(0.1x) \\
&+ \left[(-0.005C_S m_2^L n_2^L - 0.005C_S m_2^R n_2^R - 0.01C_T m_3^L n_2^L - 0.01C_T m_3^R n_2^R)\ell^2 \right] \cos(0.1y) \\
&+ \left[(0.7m_1^L n_1^L + 0.7m_1^R n_1^R + 0.7m_2^L n_2^L + 0.7m_2^R n_2^R)\mu_S + 0.7m_3^L n_3^L \mu_L + 0.7m_3^R n_3^R \mu_L \right] \cos(0.1z),
\end{aligned}
\tag{B13}
$$

where $\mathbf{n} = (n_1, n_2, n_3)^T$.

References

1. Brezzi F., Fortin M.. *Mixed and hybrid finite element methods*. Springer Science & Business Media; 2012.
2. Engel Gerald, Garikipati Krishna, Hughes TJR, Larson MG, Mazzei Luca, Taylor Robert L. Continuous/discontinuous finite element approximations of fourth-order elliptic problems in structural and continuum mechanics with applications to thin beams and plates, and strain gradient elasticity. *Computer Methods in Applied Mechanics and Engineering*. 2002;191(34):3669–3750.
3. Amanatidou E, Aravas N. Mixed finite element formulations of strain-gradient elasticity problems. *Computer Methods in Applied Mechanics and Engineering*. 2002;191(15-16):1723–1751.
4. Feng Xiaobing, Prohl Andreas. Error analysis of a mixed finite element method for the Cahn-Hilliard equation. *Numerische Mathematik*. 2004;99(1):47–84.
5. Belytschko T., Chen J.S.. Meshfree and Particle Methods. John Wiley & Sons, Ltd. 2007.
6. Huerta Antonio, Belytschko Ted, Fernandez-Mendez Sonia, Rabczuk Timon, Zhuang Xiaoying, Arroyo Marino. Meshfree Methodsch. 3. John Wiley & Sons, Ltd. 2017.
7. Cottrell J Austin, Hughes Thomas JR, Bazilevs Yuri. *Isogeometric analysis: toward integration of CAD and FEA*. John Wiley & Sons; 2009.
8. Codony David, Marco Onofre, Fernández-Méndez Sonia, Arias Irene. An Immersed Boundary Hierarchical B-spline method for flexoelectricity. *Computer Methods in Applied Mechanics and Engineering*. 2019;.
9. Nitsche J. Über ein Variationsprinzip zur LBsung van Dirichlet–Problemen bei Verwendung van Teilrümen, die keinen Handbedingungen unterworfen sind. In: :1970–1971; 1970.

10. Fernández-Méndez Sonia, Huerta Antonio. Imposing essential boundary conditions in mesh-free methods. *Computer methods in applied mechanics and engineering.* 2004;193(12-14):1257–1275.

11. Jiang Wen, Annavarapu Chandrasekhar, Dolbow John E, Harari Isaac. A robust Nitsche's formulation for interface problems with spline-based finite elements. *International Journal for Numerical Methods in Engineering.* 2015;104(7):676–696.

12. Dolbow John, Harari Isaac. An efficient finite element method for embedded interface problems. *International journal for numerical methods in engineering.* 2009;78(2):229–252.

13. Yudin PV, Tagantsev AK. Fundamentals of flexoelectricity in solids. *Nanotechnology.* 2013;24(43):432001.

14. Nguyen Thanh D, Mao Sheng, Yeh Yao-Wen, Purohit Prashant K, McAlpine Michael C. Nanoscale flexoelectricity. *Advanced Materials.* 2013;25(7):946–974.

15. Zubko Pavlo, Catalan Gustau, Tagantsev Alexander K. Flexoelectric effect in solids. *Annual Review of Materials Research.* 2013;43.

16. Krichen Sana, Sharma Pradeep. Flexoelectricity: a perspective on an unusual electromechanical coupling. *Journal of Applied Mechanics.* 2016;83(3).

17. Wang Bo, Gu Yijia, Zhang Shujun, Chen Long-Qing. Flexoelectricity in solids: Progress, challenges, and perspectives. *Progress in Materials Science.* 2019;106:100570.

18. Mocci A., Barceló-Mercader J., Codony D., Arias I.. Geometrically polarized architected dielectrics with effective piezoelectricity. *under review.* 2021;.

19. Codony D., Mocci A., Arias I.. Wheel-shaped and helicoidal torsional flexoelectric devices. *In preparation.* 2021;.

20. Mao Sheng, Purohit Prashant K, Aravas Nikolaos. Mixed finite-element formulations in piezoelectricity and flexoelectricity. *Proceedings of the Royal Society A: Mathematical, Physical and Engineering Sciences.* 2016;472(2190):20150879.

21. Deng Feng, Deng Qian, Yu Wenshan, Shen Shengping. Mixed finite elements for flexoelectric solids. *Journal of Applied Mechanics.* 2017;84(8).

22. Furihata Daisuke. A stable and conservative finite difference scheme for the Cahn-Hilliard equation. *Numerische Mathematik.* 2001;87(4):675–699.

23. Alessandroni Silvio, Andreaus Ugo, Dell'Isola Francesco, Porfiri Maurizio. Piezo-electromechanical (pem) kirchhoff–love plates. *European Journal of Mechanics-A/Solids.* 2004;23(4):689–702.

24. Ventura Jordi, Codony David, Fernández-Méndez Sonia. A C0 interior penalty finite element method for flexoelectricity. *Journal of Scientific Computing.* 2020;in press.

25. Abdollahi Amir, Peco Christian, Millan Daniel, Arroyo Marino, Arias Irene. Computational evaluation of the flexoelectric effect in dielectric solids. *Journal of Applied Physics.* 2014;116(9):093502.

26. Zhuang Xiaoying, Nanthakumar SS, Rabczuk Timon. A meshfree formulation for large deformation analysis of flexoelectric structures accounting for the surface effects. *Engineering Analysis with Boundary Elements.* 2020;120:153–165.

27. Abdollahi Amir, Millán Daniel, Peco Christian, Arroyo Marino, Arias Irene. Revisiting pyramid compression to quantify flexoelectricity: A three-dimensional simulation study. *Physical Review B.* 2015;91(10):104103.

28. Abdollahi Amir, Arias Irene. Constructive and destructive interplay between piezoelectricity and flexoelectricity in flexural sensors and actuators. *Journal of Applied Mechanics.* 2015;82(12).

29. Ghasemi Hamid, Park Harold S, Rabczuk Timon. A level-set based IGA formulation for topology optimization of flexoelectric materials. *Computer Methods in Applied Mechanics and Engineering.* 2017;313:239–258.

30. Lifshitz EM, Landau LD. *Statistical Physics (Course of Theoretical Physics, Volume 5).* 1984.

31. Sharma ND, Landis CM, Sharma P. Piezoelectric thin-film superlattices without using piezoelectric materials. *Journal of Applied Physics.* 2010;108(2):024304.

32. Landau Lev Davidovich, Lifshitz Evgenii Mikhailovich. *Course of theoretical physics*. Elsevier; 2013.

33. Liu Liping. An energy formulation of continuum magneto-electro-elasticity with applications. *Journal of the Mechanics and Physics of Solids.* 2014;63:451 - 480.

34. Codony David, Gupta Prakhar, Marco Onofre, Arias Irene. Modeling flexoelectricity in soft dielectrics at finite deformation. *Journal of the Mechanics and Physics of Solids.* 2021;146:104182.

35. Mao Sheng, Purohit Prashant K.. Insights Into Flexoelectric Solids From Strain-Gradient Elasticity. *ASME Journal of Applied Mechanics.* 2014;81(8):1–10.

36. Annavarapu Chandrasekhar, Hautefeuille Martin, Dolbow John E. Stable imposition of stiff constraints in explicit dynamics for embedded finite element methods. *International Journal for Numerical Methods in Engineering.* 2012;92(2):206–228.

37. Kolpakov AG. Calculation of the characteristics of thin elastic rods with a periodic structure. *Journal of Applied Mathematics and Mechanics.* 1991;55(3):358–365.

38. Hassani Behrooz, Hinton Ernest. A review of homogenization and topology optimization I—homogenization theory for media with periodic structure. *Computers & Structures.* 1998;69(6):707–717.

39. Barceló-Mercader J., Codony D., Fernández-Méndez S., Arias I.. Generalized periodicity for flexoelectric boundary value problems. *In preparation.* 2021;.

40. Boor C.. *A Practical Guide to Splines*. Applied Mathematical SciencesSpringer New York; 2001.

41. Marco Onofre, Sevilla Ruben, Zhang Yongjie, Ródenas Juan José, Tur Manuel. Exact 3D boundary representation in finite element analysis based on Cartesian grids independent of the geometry. *International Journal for Numerical Methods in Engineering.* 2015;103(6):445–468.

42. Marco Onofre, Ródenas Juan José, Navarro-Jiménez José Manuel, Tur Manuel. Robust h-adaptive meshing strategy considering exact arbitrary CAD geometries in a Cartesian grid framework. *Computers & Structures.* 2017;193:87–109.

43. Hoang Tuong, Verhoosel Clemens V, Auricchio Ferdinando, Brummelen E Harald, Reali Alessandro. Mixed isogeometric finite cell methods for the stokes problem. *Computer Methods in Applied Mechanics and Engineering.* 2017;316:400–423.

44. Burman Erik. Ghost penalty. *Comptes Rendus Mathematique.* 2010;348(21-22):1217–1220.

45. Höllig Klaus, Reif Ulrich, Wipper Joachim. Weighted extended B-spline approximation of Dirichlet problems. *SIAM Journal on Numerical Analysis.* 2001;39(2):442–462.

46. Höllig Klaus, Hörner Jörg, Hoffacker Axel. Finite element analysis with B-splines: weighted and isogeometric methods. In: :330–350Springer; 2012.

47. Rüberg Thomas, Cirak F. Subdivision-stabilised immersed b-spline finite elements for moving boundary flows. *Computer Methods in Applied Mechanics and Engineering.* 2012;209:266–283.

48. Rüberg Thomas, Cirak Fehmi, García Aznar José Manuel. An unstructured immersed finite element method for nonlinear solid mechanics. *Advanced Modeling and Simulation in Engineering Sciences.* 2016;3(1):22.

49. Schillinger Dominik, Ruess Martin. The Finite Cell Method: A review in the context of higher-order structural analysis of CAD and image-based geometric models. *Archives of Computational Methods in Engineering.* 2015;22(3):391–455.

50. Fernández-Méndez Sonia, Huerta Antonio. Imposing essential boundary conditions in mesh-free methods. *Computer methods in applied mechanics and engineering.* 2004;193(12):1257–1275.

51. Schillinger Dominik, Harari Isaac, Hsu Ming-Chen, et al. The non-symmetric Nitsche method for the parameter-free imposition of weak boundary and coupling conditions in immersed finite elements. *Computer Methods in Applied Mechanics and Engineering.* 2016;309:625–652.

52. Badia Santiago, Verdugo Francesc, Martín Alberto F. The aggregated unfitted finite element method for elliptic problems. *Computer Methods in Applied Mechanics and Engineering.* 2018;336:533–553.

53. Embar Anand, Dolbow John, Harari Isaac. Imposing Dirichlet boundary conditions with Nitsche's method and spline-based finite elements. *International journal for numerical methods in engineering.* 2010;83(7):877–898.

54. Griebel Michael, Schweitzer Marc Alexander. A particle-partition of unity method part V: boundary conditions. In: Springer 2003 (pp. 519–542).

55. Laursen Tod A, Puso Michael A, Sanders Jessica. Mortar contact formulations for deformable–deformable contact: past contributions and new extensions for enriched and embedded interface formulations. *Computer methods in applied mechanics and engineering.* 2012;205:3–15.

56. Annavarapu Chandrasekhar, Hautefeuille Martin, Dolbow John E. A robust Nitsche's formulation for interface problems. *Computer Methods in Applied Mechanics and Engineering.* 2012;225:44–54.

57. Sharma N.D., Landis C.M., Sharma P.. Piezoelectric thin-film superlattices without using piezoelectric materials. *Journal of Applied Physics.* 2010;108(2):1–25.

58. Sharma ND, Maranganti Ravi, Sharma P. On the possibility of piezoelectric nanocomposites without using piezoelectric materials. *Journal of the Mechanics and Physics of Solids.* 2007;55(11):2328–2350.

59. Mindlin R. D., Eshel N. N.. On first strain-gradient theories in linear elasticity. *International Journal of Solids and Structures.* 1968;4(1):109–124.

60. Altan B S, Aifantis E C. On some aspects in the special theory of gradient elasticity. *Journal of the Mechanical Behavior of Materials.* 1997;8(3):231–282.